BRAIN
ORIGINAL ARTICLE

Functional reconstruction of the basal ganglia neural circuit by human striatal neurons in hypoxic–ischaemic injured brain

Xiaoli Ji,[1,†] Yingying Zhou,[2,3,†] Qinqin Gao,[2] Hui He,[2,3] Ziyan Wu,[2] Ban Feng,[2] Yuting Mei,[1] Yan Cheng,[1] Wenhao Zhou,[4] Yuejun Chen[2,5] and Man Xiong[6]

[†]These authors contributed equally to this work.

Perinatal hypoxic–ischaemic encephalopathy is the leading cause of neonatal death and permanent neurological deficits, while the basal ganglia is one of the major nuclei that is selectively and greatly affected in the brains of hypoxic–ischaemic encephalopathy patients, especially in severe cases. Human embryonic stem cell-derived neurons have shown great potential in different types of brain disorders in adults. However, it remains unknown whether and how grafted human embryonic stem cell-derived neurons can repair immature brains with hypoxic–ischaemic encephalopathy.

Here, by administrating genetically labelled human embryonic stem cell-derived striatal neural progenitors into the ipsilateral striatum of hypoxic–ischaemic encephalopathy-injured mice, we found that the grafted cells gradually matured into GABA spiny projection neurons morphologically and electrophysiologically, and significantly rescued the area loss of hypoxic–ischaemic encephalopathy-injured brains. Intriguingly, using immunohistochemical staining combined with enhanced ascorbate peroxidase-based immunoelectron microscopy and rabies virus-mediated trans-synaptic tracing, we show that the grafts start to extend axonal projections to the endogenous target areas (globus pallidus externa, globus pallidus internus, substantia nigra), form synapses with host striatal, globus pallidus and nigra neurons, and receive extensive and stable synaptic inputs as early as 2 months post-transplantation. Importantly, we further demonstrated functional neural circuits re-established between the grafted neurons and host cortical, striatal and substantial nigra neurons at 3–6 months post-transplantation in the hypoxic–ischaemic encephalopathy-injured brain by optogenetics combined with electrophysiological recording. Finally, the transplanted striatal spiny projection neurons but not spinal GABA neurons restored the motor defects of hypoxic–ischaemic encephalopathy, which were reversed by clozapine-*N*-oxide-based inhibition of graft function.

These findings demonstrate anatomical and functional reconstruction of the basal ganglia neural circuit including multiple loops by striatal spiny projection neurons in hypoxic–ischaemic encephalopathy-injured immature brains, which raises the possibility of such a cell replacement therapeutic strategy for hypoxic–ischaemic encephalopathy in neonates.

1 Stem Cell Center, Children's Hospital of Fudan University, Shanghai 201102, China
2 Institute of Neuroscience, State Key Laboratory of Neuroscience, CAS Center for Excellence in Brain Science and Intelligence Technology, Chinese Academy of Sciences, Shanghai 200031, China
3 University of Chinese Academy of Sciences, Beijing, China
4 Key Laboratory of Neonatal Diseases of National Health Ministry, Children's Hospital, MOE Frontiers Center for Brain Science, Fudan University, Shanghai 200032, China
5 Shanghai Center for Brain Science and Brain-Inspired Intelligence Technology, Shanghai, China

Received April 11, 2022. Revised August 16, 2022. Accepted September 09, 2022

6 State Key Laboratory of Medical Neurobiology and MOE Frontiers Center for Brain Science, Institutes of Brain Science, Stem Cell Center of Children's hospital, Fudan University, Shanghai 200032, China

Correspondence to: Man Xiong
138 Medical College Road, Shanghai, Fudan University, China
E-mail: man_xiong@fudan.edu.cn

Correspondence may also be addressed to: Yuejun Chen
320 Yueyang Road, Chinese Academy of Sciences, Shanghai, China
E-mail: yuejunchen@ion.ac.cn

Wenhao Zhou
399 Wanyuan Road, Children's Hospital of Fudan University, Shanghai, China
E-mail: wenhaozhou@fudan.edu.cn

Keywords: human embryonic stem cell; stem cell transplantation; hypoxic–ischaemic encephalopathy; neural circuit reconstruction; striatal spiny projection neuron

Introduction

Despite recent improvements in perinatal and neonatal intensive care medicine, hypoxic–ischaemic encephalopathy (HIE) remains the leading cause of mortality and long-term neurological sequelae, such as mental retardation, cerebral palsy and lifelong cognitive and motor disabilities in neonates.[1–4] Stem cell-based therapies hold great promise as potential novel treatments to restore brain function after HIE.[5] Transplantation of different types of multipotent stem cells, such as mesenchymal stem cells and umbilical cord blood stem cells, have been shown to have preliminary positive effects in animal models.[6–9] However, the therapeutic effects of these donor cells are thought to stem from the bystander effects with possible mechanisms, including neuroprotection and immunomodulation.[10] Evidence of cell replacement therapy by human pluripotent stem cell (hPSC)-derived neurons, especially neural circuit repair by grafted neurons, which is probably the most promising strategy to restore functionality efficiently and long-term in the injured immature brain, is virtually lacking.

During neonatal hypoxic–ischaemic injury, an insufficient supply of oxygen (hypoxia) and/or poor blood flow (ischaemia) reaching a particular area of the newborn brain leads to a large number of neuronal deaths triggered by the activation of various neurotoxic molecules and death pathways.[1,11,12] Previous MRI and post-mortem studies have demonstrated selective vulnerability and neuronal loss in the sensorimotor cortex, basal ganglia, thalamus and brain stem in infants with severe HIE.[13,14] The lesion severity of the basal ganglia, where the striatum is the major nucleus, was found to be strongly associated with the severity of motor impairment in full-term infants with HIE.[15,16] On the other hand, in HIE animal models, striatal GABA spiny projection neurons, which make up 95% of all striatal neurons and project to both the globus pallidus (GP) and the substantia nigra (SN), but not GABA interneurons, appear to be severely affected.[17,18] This evidence strongly indicates the great potential of striatal GABA spiny projection neurons as therapeutic target cells to restore the functionality of neonates with HIE.

Currently, brain region-specific human neural progenitor cells (hNPCs), such as cortical or striatal neural progenitors (SNPs), have been successfully differentiated from hPSCs.[19–21] These hNPCs have been proven to differentiate into functional neurons and incorporate into adult host cortical neural circuitry to regulate motor behaviour in stroke mice[22,23] or restore target tissue activity in Huntington's disease animals.[24] We have recently reported that transplanted hPSC-derived dopaminergic neurons anatomically and functionally repaired the nigra–striatal circuit of Parkinson's disease animals.[25] These studies indicate the neural circuit repairing capacity of hPSC-derived neural progenitors in the adult diseased brain. Nevertheless, the high plasticity of the immature brain and massive neuronal loss accompanied by extensive astrocyte activation causing enhanced production of axonal regeneration inhibition molecules such as chondroitin sulphate proteoglycans[26,27] and late onset of apoptosis entangled with microglial activation and macrophage invasion lasting for several weeks in the HIE-injured immature brain provide a more complicated microenvironment for the survival and integration of grafted human cells in the host brain in comparison with others.[28,29]

Given the striatum is the main input nucleus receivings excitatory afferents from the cortex and forming the origin of indirect (striatum to globus pallidus externa, GPe) and direct (striatum to globus pallidus internus, GPi, and SN) pathways, two major pathways of basal ganglia circuit involved in motor control,[30] repairment of this circuit is probably the best way to rescue motor defects in HIE patients. Here, we found obvious ipsilateral striatal neuron loss accompanied by motor function impairment in an HIE-injured mouse. By transplantation of striatal neural progenitors derived from human embryonic stem cells (hESCs) into the striatum of HIE-injured mouse brains, we found that the grafted cells largely differentiated into striatal GABA spiny projection neurons and significantly rescued the area loss of HIE-injured brains. More importantly, these grafted spiny projection neurons projected to the striatal endogenous target regions GP (GPe, GPi) and SN (substantia nigra reticulate, SNr, and substantia nigra compacta, SNc), formed synaptic connections with host neurons and received extensive synaptic inputs from host neurons, thereby reconstructing the indirect and direct pathways of basal ganglia anatomically. Furthermore, the grafted neurons functionally incorporated into the host basal ganglia neural circuit and rescued the motor deficits of HIE-injured animals in the long term. Our data demonstrate for the first time that the anatomy and function of damaged basal

ganglia neural circuits in the HIE-injured brain can be reconstructed by transplantation of striatal spiny projection neurons, which provides strong evidence for stem cell replacement therapy for the treatment of hypoxic–ischaemic immature brain injury.

Materials and methods

Cell culture

hESCs [line WA09 (WiCell), passages 20–40] and gene editing cell lines from hESCs were maintained on a feeder layer of irradiated mouse embryonic fibroblasts (MEFs) in hESCs medium consisting of Dulbecco's modified Eagle Medium/Nutrient Mixture F-12 (DMEM/F-12), 1×GlutaMAX, 1×non-essential amino acids (NEAA) and 0.1 mM β-mercaptoethanol (reagent information is given in Supplementary Table 1).

Cell line construction

H9 hESCs were pretreated with rho-kinase (ROCK) inhibitor (0.5 μM), digested into single cells by TrypLE™ Express Enzyme and then electroporated with the appropriate combination of Cas9 plasmids, sgRNA and donor plasmids in 500 μl of electroporation buffer (5 mM KCl, 5 mM $MgCl_2$, 15 mM HEPES, 102.94 mM Na_2HPO_4 and 47.06 mM NaH_2PO_4, pH = 7.2) using the Gene Pulser Xcell System (Bio-Rad) at 250 V and 500 mF in a 0.4 cm cuvette (Phenix Research Products). Cells were then seeded onto MEFs in six-well plates in MEF-conditioned embryonic stem cell (ESC) culture medium (CM). Seventy-two hours later, puromycin (0.5 mg/ml) or G418 (50–100 mg/ml) was added to the CM for selection for 2 weeks. Individual clones were picked up after drug selection, and the integration of the transgene was identified by genomic PCR. For the generation of iCre, mCherry, ChR2-EYFP and hM4Di-mCherry knock-in hESCs, the iCre, mCherry, ChR2-EYFP or hM4Di-mCherry expression cassette was inserted into the *AAVS1* locus of H9 hESCs.

Generation of striatal GABA projection neurons and spinal GABA neurons

Striatal neural progenitors were differentiated from hESCs with a modified protocol following a previous report.[20] Briefly, hESCs on MEFs (5–6 days after passaging) were digested into small clumps with dispase and cultured with ESC medium without basic fibroblast growth factor (bFGF) in a T25 flask for 3 days to form embryonic bodies (EBs). The cultured medium was changed every day. From Day 4 to Day 6, EBs were induced to neuroepithelium with SB431542 (2 μM) and DMH-1 (2 μM) in neural induction medium (NIM) including DMEM/F-12, 1× N2 supplement and 1× NEAA. On Day 7, neural spheres were attached to six-well plates in NIM containing 5% foetal bovine serum for 20 h, then the medium was changed with NIM every other day until Day 10. From Day 10 to Day 15, SAG (0.2 μM), which is an agonist of the sonic hedgehog pathway, was added to the NIM medium. On Day 16, the neural rosettes on six-well plates were blown off slightly with 1 ml tips and cultured with ROCK inhibitor (0.5 μM), SAG (0.2 μM) and 1×B27 in a T25 flask. From Day 17 to Day 26, cells were kept in 25 ml flask feeding with NIM (0.2 μM SAG), which was changed every other day. To generate spinal GABA neurons, all procedures are the same as the differentiation of striatal neural progenitors except 0.1 μM retinoic acid (RA) was added into the NIM from Day 10 to Day 23.[31] For neuron maturation *in vitro*, neurospheres were dissociated with Accutase at Day 27 and then placed onto polyornithine- and matrigel-coated coverslips in neural differentiation medium (NDM), including Neurobasal™ medium, 1×N2 supplement, 1×B27, supplemented with brain-derived neurotrophic factor (BDNF, 20 ng/ml), glial-derived neurotrophic factor (GDNF, 10 ng/ml), insulin-like growth factor 1 (IGF1, 10 ng/ml), cylic adenosine monophosphate (cAMP, 1 μM), ascorbic acid (AA, 200 μM) and Compound E (0.2 μM). The coverslips are fixed for immunostaining after maturation for 2 weeks.

HIE mouse model and brain injury assessment

This study was conducted in accordance with the National Institute of Health Guide for the Care and Use of Laboratory Animals, and all protocols were approved by the Shanghai Committee on Ethics in the Care and Use of Laboratory Animals. Animals were maintained on a 12-h light/12-h dark cycle and had free access to food and water throughout the study. The HIE model was induced in the mouse at postnatal Day 7, as described previously.[32] Briefly, the left common carotid artery of severe combined immunodeficiency (SCID) mice was isolated, double ligated with 5–0 surgical silk and then occluded permanently under isoflurane anaesthesia. The surgical procedure was performed in less than 5 min. After being returned to the dam to recover for 2 h, pups were exposed to hypoxia at 36.5–37.0°C thermostat, which perfused with a humidified gas mixture (8% oxygen in nitrogen) for 30 or 60 min. Sham-control animals underwent the same procedures without occlusion of the artery. To assess brain injury in SCID mice, mice were euthanized 7 days post-HIE surgery. Animals were perfused transcardially with 0.9% saline followed by 4% paraformaldehyde (PFA) for fixation. After sequential dehydration in 20 and 30% sucrose, 30-μm brain sections were obtained by a microtome and stored at −20°C in cryoprotectant solution for further experiments. For cresyl violet (CV) staining, brain slices (30 μm) were placed on gelatine-coated glass slides and baked for 2 h at 37°C. Then, brain slices were dehydrated in 75%, 85%, 95% (twice) and 100% (twice) ethanol for 8 min for each step, followed by immersion in 95%, 85%, 75%, 50% ethanol for 3 min for each step. After a quick rinse in distilled water, the brain slices were immersed in CV staining solution for 10–15 min. Then, the stained slices were quickly rinsed in 75%, 85%, 95% (0.3% glacial acetic acid) and 100% (twice) ethanol. After the transparent process by soaking in ethanol/xylene (1:1) and xylene (twice) for 10 min for each step, slices were sealed with neutral resin. To assess the brain area loss caused by HIE injury, CV-stained sections (every sixth section) were imaged by a 20× objective with an Olympus microscope (Olympus VS120). Brain area loss was measured by ImageJ and calculated as the (area of contralateral hemisphere − area of ipsilateral hemisphere) × 100% / area of contralateral hemisphere).

Cell transplantation and immunostaining

Striatal or spinal neural progenitors were digested into very small clusters at Day 32 and kept in NIM medium for another 2 days, and then small clusters of neural progenitors were transplanted at Day 34. Briefly, animals were randomly grouped and placed into a stereotaxic apparatus 2 weeks after HIE surgery. Two microlitres of cell suspension in artificial cerebrospinal fluid (ACSF) containing 1× B27, BDNF (20 ng/ml), and ROCK inhibitor (0.5 μM) was stereotaxically injected into the ipsilateral dorsal striatum using a needle affixed to a syringe pump at the following coordinates (AP: +0.8 mm; ML: +1.7 mm; DV: −3.2 mm from dura). The injection procedure took 10 min. Age-matched mice that underwent the same HIE procedure but received ACSF only served as controls.

For immunohistochemical staining, brain slices were incubated in blocking solution (10% donkey serum and 0.3% Triton

X-100 in Dulbecco's PBS (DPBS)) for 1 h and then incubated with primary antibodies including hNCAM, GABA, DARPP32, CTIP2, GFAP, SST, CR, Ki67 and hN (antibody information is given in Supplementary Table 1) at 4°C for 1–3 nights. The unbound primary antibodies were washed with DPBS. For fluorescent immunostaining, slices were incubated with corresponding fluorophore-conjugated secondary antibodies for 1 h at room temperature. Nuclei were stained with Hoechst 33342 and slices were mounted in Fluoromount-G. Images were acquired using a Nikon TIE A1 plus confocal microscope. For diaminobenzidine (DAB) staining, slices were incubated with biotinylated secondary antibodies for 1 h and then incubated with avidin–biotin peroxidase for 1 h at room temperature. Immunoreactivity was observed with DAB-reaction product. For quantification of the human fibre density, we selected three representative coronal planes for each brain region, bregma −0.34 mm, −0.46 mm, −0.58 mm for GPe; bregma −1.22 mm, −1.34 mm, −1.46 mm for GPi; bregma −2.92 mm, −3.08 mm, −3.16 mm for SNc and SNr according to the mouse brain atlas. Brightfield images of the DAB staining were captured by a 20× objective with an Olympus microscope (Olympus VS120).

Whole-cell patch-clamp and brain slice recording

Coronal brain slices (300 μm) were prepared from animals at 2 and 6 months post-transplantation (MPT) using a vibratome (Leica VT1200S). Slices were incubated in solution containing oxygenated (95% O_2 and 5% CO_2) ACSF containing (in mM): 124 NaCl, 4.4 KCl, 2 $CaCl_2$, 1 $MgSO_4$, 25 $NaHCO_3$, 1 NaH_2PO_4 and 10 glucose at room temperature for 60 min. Current and voltage signals were recorded by an Axon 700B amplifier (Axon). Current and optogenetic stimulation-induced action potentials (APs) of grafted cells were recorded in current clamp mode. Electrodes were filled with a solution containing (in mM): 120 K-gluconate, 5 NaCl, 1 $MgCl_2$, 0.2 EGTA, 10 HEPES, 2 Mg-ATP, 0.1 Na_3-GTP and 10 phosphocreatine disodium, adjusted to pH 7.2 with HCl. APs were detected in response to depolarizing currents (0–100 pA, step 10 pA, duration 400 ms) or blue light illumination (470 nm, 2 ms, 5 Hz, duration 1000 ms 1.5 mW/mm^2) in current clamp mode. The spontaneous excitatory postsynaptic currents (sEPSCs), spontaneous inhibitory postsynaptic currents (sIPSCs) and optogenetic stimulation of channelrhodopsin 2 (ChR2)-expressing inputs were recorded in voltage clamp mode. Electrodes were filled with a solution containing (in mM) 112 Cs-Gluconate, 5 TEA-Cl, 3.7 NaCl, 0.2 EGTA, 10 HEPES, 2 Mg ATP, 0.3 Na_3GTP and 5 QX-314 (adjusted to pH 7.2 with CsOH). Optogenetic stimulation of ChR2-expressing inputs was achieved with wide-field illumination using a blue LED (470 nm, 2 ms, 1.5 mW/mm^2). Data were analysed offline with Clamfit and MiniAnalysis. In all cases, biocytin (0.4%) was added to the internal solution to identify the morphological properties of the recorded cells.

Viral injection and rabies-mediated tracing

For rabies-mediated tracing experiments, 200 nl adeno-associated virus (AAV) expressing Cre-dependent TVA and tdTomato with a nuclear location signal (NLS-tdTomato) [AAV-DIO-TVA-2A-NLS-tdTomato, titre 1.29×10^{12} genome copies (gc)/ml] and 200 nl AAV expressing Cre-dependent rabies glycoprotein [AAV-DIO-G (DIO, double-floxed invertedorientation; G, glycoprotein), titre 1.29×10^{12} gc/ml] were coinjected into the grafted site (AP: +0.8 mm; ML: +1.7 mm; DV: −3.2 mm from dura) of HIE mice 1 or 5 months after transplantation. Three weeks later, EnvA-pseudotyped and G-deleted rabies virus-tagged enhanced green fluorescent protein (EGFP) (RVdG-EGFP, 400 nl, titre 2×10^8 pfu/ml) was injected into the same site. One week later, the mice were perfused and sliced coronally. To quantify presynaptic inputs to graft from different brain regions of the ipsilateral, serial slices (30 μm, every fourth) of total brain without staining were captured directly by a 20× objective with a fluorescence microscope (Olympus VS120). The outline of brain areas and the distribution of the traced neurons were manually labelled using Photoshop software according to the mouse brain atlas. Quantification and comparison of the percentage of ipsilateral inputs were done by a blinded counter. Some brain slices were performed immunohistochemistry staining to elucidate the cell identity.

Immunoelectron microscopy

A total of 400 nl AAV expressing Cre-dependent (DIO) enhanced ascorbate peroxidases 2 (APEX2) with a nuclear export signal (AAV-DIO-APEX2-NES, titre 9.86×10^{12} g/ml) was injected into the grafted site (AP: +0.8 mm; ML: +1.7 mm; DV: −3.2 mm from dura) of HIE-injured mouse brains at 5 MPT. Three weeks later, the mice were prepared for immunoelectron microscopy. Briefly, animals were perfused transcardially with 0.9% saline and then fixed with 4% PFA combined with 0.8% glutaraldehyde. Brain slices (100 μm) were sectioned by a vibratome, fixed in the abovementioned fixative for 4 h and then reacted with DAB solution to reveal sites of peroxidase activity. The slices were rinsed with 0.1 M ice-cold Tris–HCl (pH = 7.40) and fixed with 1% OsO_4 for 1 h. Then, the slices were rinsed in 0.1 M phosphate buffer, dehydrated in 50%, 70%, 80%, 90% and three steps of 100% ethanol followed by propylene oxide and embedded in Epon. To identify the APEX2-labelled synapses, ultrathin sections were cut and counterstained with lead citrate and uranyl acetate. Ultrathin sections were mounted on grids, examined and photographed using a transmission electron microscope JEM-100CX (JEOL). Synapses were defined by the presence of synaptic vesicles in a presynaptic terminal, a postsynaptic density in postsynaptic structure and synaptic cleft.

Imaging and cellular quantification

For neural differentiation *in vitro*, to quantify the population of GABA/Meis2, DAPPP32 and GABA/CTIP2-immunopositive cells, at least four randomly chosen images from coverslips were manually counted by a blinded counter using ImageJ software. Neural differentiation experiment was replicated for three times and data. For *in vivo* graft characterization, serial sections (30 μm, every sixth section between 1.20 mm and −0.20 mm from the bregma) from the graft were used to stain by GABA, DARPP32, CTIP2, GFAP, SST, CR, Ki67, hN for stereological quantification. The graft was outlined and captured by a 20× objective with Nikon TIE A1 plus confocal microscope. Single- or double-stained cells were counted manually by a blinded counter with ImageJ. For quantification of the human fibre optical density, images of human neural cell adhension molecule (hNCAM$^+$) fibres were acquired by a Nikon TIE A1 plus confocal microscope. The optical density of hNCAM$^+$ fibres in the GP and SN of the mouse brain was measured by a blinder counter using ImageJ following the automated threshold. All data are presented as mean ± SEM.

Behavioural tests

Three behavioural tests were chosen to evaluate the motor recovery of HIE mice at 2, 4 and 6 MPT. For the chemical-control behavioural test, animals were recorded 20 min after intraperitoneal injection of clozapine-*N*-oxide (CNO; 4 mg/kg, Biomol International) or saline. All animals needed to adapt in the behaviour room for 30 min before recording. All behavioural tests were conducted by investigators blind to the mouse treatments.

Cylinder test

An individual mouse was placed in a transparent glass and recorded by a camera for 5 min. The ipsilateral and contralateral paw touching the wall of the cylinder was counted. The minimum touch number is 20 in total 5 min video were collected. Videos were analysed by investigators blind to the groups. The data were expressed as the percentage of ipsilateral touches to total touches.

Open field test

Individual mice were placed in a plastic open-field chamber (40 cm × 40 cm × 40 cm), and the distance covered was tracked and analysed using the Ethovision video tracking system (from Noldus Information Technology). Activities were recorded for 10 min under normal conditions of lighting. Quantitative analysis was done on total distance.

Rotarod test

An accelerating Rotarod (Med Associates Instruments) was used to test motor coordination. All animals were pretrained for three consecutive days in order to reach a stable performance. On Day 1, mice were trained on the rotating rod at speed of 5 rpm in a period of 300 s three times. On Day 2 and Day 3, mice were trained on rod accelerating from 5 to 40 rpm within 60 s in a period of 300 s three times. A formal test was performed from the fourth day. The time each mouse stayed on the rotating rod was recorded, and the average duration from three repeated tests of each animal was used for data analysis.

Statistical analyses

SPSS version 20.0 was used for statistical analysis. The results were analysed using Student's *t*-test, one-way ANOVA or two-way ANOVA followed by Tukey's multiple comparison test. $^{*}P < 0.05$, $^{**}P < 0.01$, $^{***}P < 0.001$ were considered to be significant.

Data availability

Data that support the findings of this study are available from the corresponding author on reasonable request.

Results

HESC-derived SNPs mature into striatal GABA spiny projection neurons and rescue brain area loss in HIE-injured brains

To test hESC-based cell therapy for HIE-injured immature brains, we designed an experimental procedure, as shown in Fig. 1A. To generate an HIE model using SCID mice, we investigated 30 min and 1 h durations of hypoxic exposure, which will affect animal survival and the severity of brain injury after ligation of the left common artery at postnatal Day 7. The results showed that 1 h of hypoxic exposure caused high mortality (66 ± 9.0%) with massive brain tissue loss (Supplementary Fig. 1A–C), while 30 min of hypoxic exposure resulted in moderate mortality (28.27 ± 2.85%; Supplementary Fig. 1A) with relatively intact brain structures but obvious shrinkage of the ipsilateral brain tissue (Fig. 1B and C). Statistical data of CV staining displayed 60.23 ± 2.71% ipsilateral brain area loss in 1 h hypoxic exposure animals in contrast to 39.47 ± 8.29% in 30 min animals (Supplementary Fig. 1F). Thus, we chose 30 min of hypoxic exposure to generate an HIE model in SCID mice in the following studies. Interestingly, further assessment of CV staining slices indicated that HIE brain injury induced a significantly larger area loss in the ipsilateral striatum (39.04 ± 3.23%) than in the cortex (21.19 ± 4.37%; Fig. 1F). The neuronal staining by NeuN and statistical analysis revealed obvious loss of neurons in the ipsilateral striatum (ipsi, white dotted lines and magnified rectangles in subpanel a, 777.08 ± 90.01) compared to the contralateral (contra, white dotted lines and magnified rectangles in subpanel b, 2316.58 ± 412.09) in the HIE-injured brain (Fig. 1D and E). In addition, we observed dramatic astrogliosis by glial fibrillary acidic protein (GFAP) (ipsi: 139.26 ± 32.80, contra: 39.07 ± 10.40; $P < 0.05$) and microglial/macrophage activation by ionized calcium binding adapter molecule 1 (Iba-1) (ipsi: 196.86 ± 45.70, contra: 51.81 ± 14.51; $P < 0.05$) in the ipsilateral brain (Supplementary Fig. 1D, E, G and H), indicating characteristics of an HIE-injured brain.[33] Overall, we successfully generated an HIE model with SCID mice, which showed obvious area and neuronal loss in the ipsilateral striatum.

We then differentiated hESCs into SNPs with a modified protocol based on a previous report.[20] Immunohistochemical staining and statistical data showed that 91.24 ± 1.03% of cells costained for GABA and Meis2 6–7 weeks after neural differentiation and maturation *in vitro*, suggesting striatal GABAergic neurons. A total of 90 ± 0.87% of cells were stained with DARPP32, a striatal GABA spiny projection neuron marker (Fig. 1G and H). In addition, we found that 60.62 ± 3.99% of cells were colabelled by GABA and CTIP2, which is an essential transcription factor for striatal GABA neurons (Fig. 1G and H). Few ChAT^{+} neurons (0.87% ± 0.14%) and GFAP^{+} cells (0.54% ± 0.10%), no neural progenitors (SOX2^{+}) or oligodendrocytes (O4^{+}) were detected at this stage in this neural differentiation system (Supplementary Fig. 2E and F). Further qPCR analysis revealed *ASCL1*, *DLX2* and *GSX2*, specific genes for lateral ganglionic eminence neural progenitors, were highly expressed in SNPs and then gradually decreased in mature neurons (Supplementary Fig. 2B). We also observed gradually increased genes for GABAergic neurons (*GABRA1* and *GAD67*), striatum GABA neuron-specific transcription factor *CTIP2*, and characteristic genes for spiny projection neurons (*DRD1* and *TAC1* for the D1 subtype, *DRD2* and *PENK* for the D2 subtype) during neural differentiation and maturation (Supplementary Fig. 2C and D). These results confirmed successful acquisition of striatal spiny projection neurons from hESCs with high purity.

To explore whether hESC-derived SNPs could survive and mature in the HIE-injured brain, we transplanted those neural progenitor cells that show high expression of neural progenitor marker SOX2 but not any ESC markers such as OCT4, NANOG and SSEA-4 into the ipsilateral striatum 2 weeks after HIE surgery (Supplementary Fig. 2A). Grafts were identified by immunofluorescent staining of GABA or DARPP32 with human nuclei hN or hN/CTIP2 at 2 and 6 MPT, respectively (Fig. 1I and K). Data quantification and analysis revealed that 34.48 ± 3.03% of transplanted cells were GABA-positive and 27.88 ± 1.85% were DARPP32-positive at 2 MPT, and this ratio increased to 78.94 ± 1.65% for GABA and 70.81

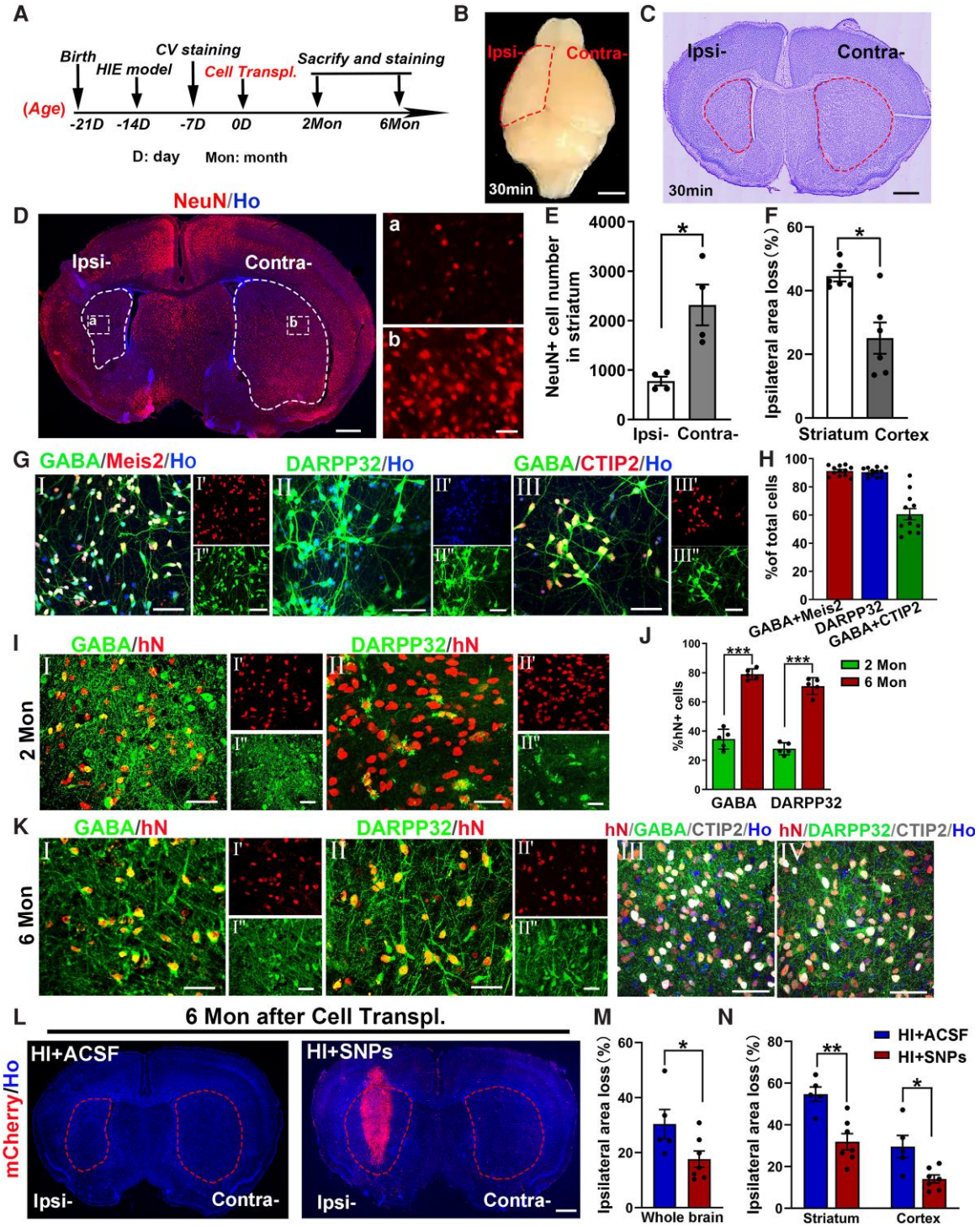

Figure 1 Transplanted hESC-derived SNPs mature into spiny projection neurons and rescue brain area loss in HIE-injured brains. (**A**) The timeline of the experimental design in this study. (**B**) Whole-mount view of mouse brain at 7 days after hypoxia–ischaemia for 30 min, scale bars = 2 mm. (**C** and **F**) Representative images of CV staining and the quantification data show obvious area loss of ipsilateral striatum and cortex in contrast to the contralateral in the HIE-injured brain. Scale bars = 500 μm. (**D** and **E**) Immunohistochemical staining and quantification of NeuN shows significant neuronal loss in the ipsilateral striatum compared with the contralateral striatum in mice with HIE injury. Scale bars = 500 μm. The boxed areas are magnified in **a** and **b**, scale bars = 100 μm. (**G** and **H**) Immunofluorescent staining and quantification of hESC-derived striatal neurons stained by $GABA^+/Meis2^+$ (**I**), $DARPP32^+$ (**II**) and $GABA^+/CTIP2^+$ (**III**) at Day 45 after neural differentiation and maturation. Scale bar = 50 μm. (**I** and **K**) Immunohistochemical images show transplanted neurons costained by hN with GABA (I) or DARPP32 (II), GABA/CTIP2 (III) or DARPP32/CTIP2 (IV) in the grafts at 2 or 6 months after transplantation. Scale bar = 25 μm. (**J**) Quantification of cellular differentiation presented in (**I**) and (**K**). (**L**) Immunostaining for mCherry+ graft 6 MPT in HIE-injured mice transplanted with ACSF or human SNPs. Scale bar = 500 μm. (**M** and **N**) Quantification of ipsilateral brain area loss grafted with ACSF or SNPs in HIE-injured mice at 6 MPT. $n = 3$ independent experiments or $n = 4$–7 mice in each group. Data are presented as the mean ± SEM. Student's *t*-test, $^*P < 0.05$, $^{**}P < 0.01$, $^{***}P < 0.001$. Ipsi- = ipsilateral; Contra- = contralateral.

±2.58% for DARPP32 at 6 MPT (Fig. 1J). Of note, most of the grafted GABA or DARPP32 immunopositive neurons coexpressed CTIP2 at 6 MPT (Fig. 1K, right). Only a small population of grafted neurons expressed somatostatin (SST) (4.54% ± 0.59%) and calretinin (CR) (5.03 ± 0.43%) for GABA interneuron, and GFAP (5.98 ± 0.75%) for astrocyte. Less than one per cent of grafted cells stained with Ki67, suggesting very few proliferated cells in the grafts at 6 MPT (Supplementary Fig. 2G and H). These data strongly support that grafted SNPs survive, differentiate and mature into striatal GABA spiny projection neurons successfully in the HIE-injured brain. More importantly, the grafted cells repopulated the injured striatum and significantly reduced the area loss of the total ipsilateral brain (17.61 ± 2.95%), ipsilateral striatum (31.87 ± 3.90%) and ipsilateral cortex (13.94 ± 1.94%) compared to the ACSF control (total ipsilateral area loss: 30.36 ± 5.33%, striatum: 54.70 ± 3.49%, cortex: 29.58 ± 5.31%) at 6 MPT, supporting hESC-derived SNPs as a potential cell source with great therapeutic effects for HIE-injured brains.

Grafted striatal neurons show functional activity in the HIE-injured striatum

To further explore the functional maturation of the grafted human SNPs, mCherry or ChR2-EYFP was knocked into the *AAVS1* locus of hESC (Fig. 2A) to specifically manipulate grafted cells after transplantation. The electrophysiological properties of transplanted cells were recorded at different time points (2, 6 MPT) by whole-cell patch-clamp recordings. Both current- or blue light-induced APs (Fig. 2B and C) and spontaneous action potentials (sAPs; Fig. 2D) showed few spikes by 2 MPT, suggesting functional immaturity of grafted cells. However, the grafted cells displayed sustained responses to current or blue light stimulation and intensive sAP with higher peak firing rates (Fig. 2E–G), which was revealed by statistically significant ($P < 0.01$) increases in spike numbers (Fig. 2H) and the light-induced AP ratio (Fig. 2I) at 6 MPT (100%) in contrast to 2 MPT (56 ± 14%). Moreover, grafted cells showed higher membrane capacitance (Cm; 2 MPT: 47.92 ± 3.34 pF, 6 MPT: 70.46 ± 8.29 pF; $P < 0.01$) and lower membrane resistance (Rm; 2 MPT: 2392.04 ± 376.40 MΩ, 6 MPT: 457.10 ± 96.22 MΩ; $P < 0.001$) and higher resting membrane potential (RMP; 2 MPT: −46.65 ± 3.62 mV, 6 MPT: −58.57 ± 1.37 MΩ; $P < 0.01$) at 6 MPT than at 2 MPT (Fig. 2J–L). These data suggest that grafted cells become functionally active and mature in the HIE-injured striatum. Interestingly, the repetitive and non-equidistant spikes displayed by current-induced APs (Supplementary Fig. 3A–D) closely resemble those of endogenous striatal spiny projection neurons in mice,[34] indicating identity of the grafted cells. No significant differences in amplitude, threshold or half-width suggested similar properties of current-induced single APs between 2 and 6 MPT (Supplementary Fig. 3E–G).

Grafted striatal neurons project to their endogenous targets in HIE-injured brains

Targeted axonal outgrowth is essential for the reconstruction of damaged neural circuits. Thus, we tested the axonal projection of the grafted SNPs derived from the hESCs-mCherry line (Fig. 3A). Compared to the contralateral, we found that many human fibres stained by hNCAM or mCherry appeared in endogenous striatal targets GPe, GPi and substantial nigra, including SNc and SNr, in the ipsilateral HIE-injured brain at 2 MPT (Fig. 3B and C). Few fibres appeared in non-target areas, such as the cortex and contralateral brain, suggesting high specificity of axon projection from the grafted SNPs in HIE-injured brains (Fig. 3B and C). To investigate the dynamic process of graft-derived neurite extension, we examined axonal outgrowth from the graft in GP (GPe and GPi) and SN (SNr and SNc) at 1, 2 and 6 MPT. The immunostaining results (Fig. 3D and E) showed that the hNCAM$^+$ fibres presented in the ipsilateral GP and SN of HIE-injured brain as early as 1 MPT, and then the human fibres gradually increased at 2 MPT and peaked by 6 MPT. The quantification of the area covered by hNCAM$^+$ fibres revealed a similar optical density of human fibres at 1 and 2 MPT, then significantly increased at 6 MPT ($P < 0.01$) in the ipsilateral GPe and GPi (Fig. 3F and G). However, for SN including SNc and SNr, the brain region far away from the graft, very few hNCAM$^+$ fibres appeared at 1 MPT, and they were dramatically elevated from 2 MPT ($P < 0.05$) until 6 MPT ($P < 0.05$ for SNc, $P < 0.01$ for SNr), compared with the earlier time points (Fig. 3H and I). These data display dynamic and successful projection of axons from grafted human SNPs to endogenous striatal targets with high specificity, suggesting anatomical reconstruction of the basal ganglia neural circuit by human SNPs in HIE-injured brains.

Grafted striatal neurons reform synapses with host neurons in the axon targeted regions of HIE-injured brains

To further investigate whether the grafted neurons could integrate into the host neural circuit, we performed double immunostaining of the human-specific presynaptic marker synaptophysin (hSYN) with host neuronal markers. The representative images show obvious GABA$^+$ synaptic puncta in the striatum, GP (GPe and GPi) and TH$^+$ synaptic puncta in the nigra, indicating the formation of synapses between grafted and host neurons (Fig. 4B–E). To specifically observe synaptic connectivity between grafts and hosts with high resolution, we transplanted SNPs differentiated from hESC lines that genetically express Cre recombinase (iCre) in the *AAVS1* site (Fig. 4A). Five months after transplantation, the grafted cells were infected with Cre-dependent AAV expressing a peroxidase derivative, APEX2, which label the cytoplasm of the grafted cells with high electron density while retaining a high-quality ultrastructure[35]; thus, the synaptic vesicles of grafted neurons could be clearly detected in presynaptic terminals. One month later, DAB immunostaining combined with electron microscope data showed axon terminals from the grafted neuron with multiple presynaptic vesicles form typical synapses with host dendritic spines, soma and axon terminals in the ipsilateral striatum and GP (GPe and GPi) of HIE-injured brain (Fig. 4F–H). Importantly, we observed axon terminals projecting from striatal grafts form synapses with host dendrite spines and axon terminals in the ipsilateral nigra of HIE-injured brains (Fig. 4I). Taken together, grafted hESC-derived striatal neurons establish synaptic connections with host neurons including proximal and distal striatal targeting brain regions, suggesting reconstruction of the host basal ganglia neural circuit anatomically in HIE-injured brains.

Grafted striatal neurons receive extensive synaptic inputs from different regions of the HIE-injured brain

To further explore whether the grafted neurons form host-to-graft synaptic connections and their upstream origins, we used monosynaptic tracing based on 'modified' EnvA-pseudotyped glycoprotein-deleted rabies virus combined with the Cre-loxP gene expression system to map direct inputs to grafted neurons (Fig. 5A). We transplanted SNPs derived from the hESC-iCre line into the ipsilateral striatum of HIE mice. One or five months after

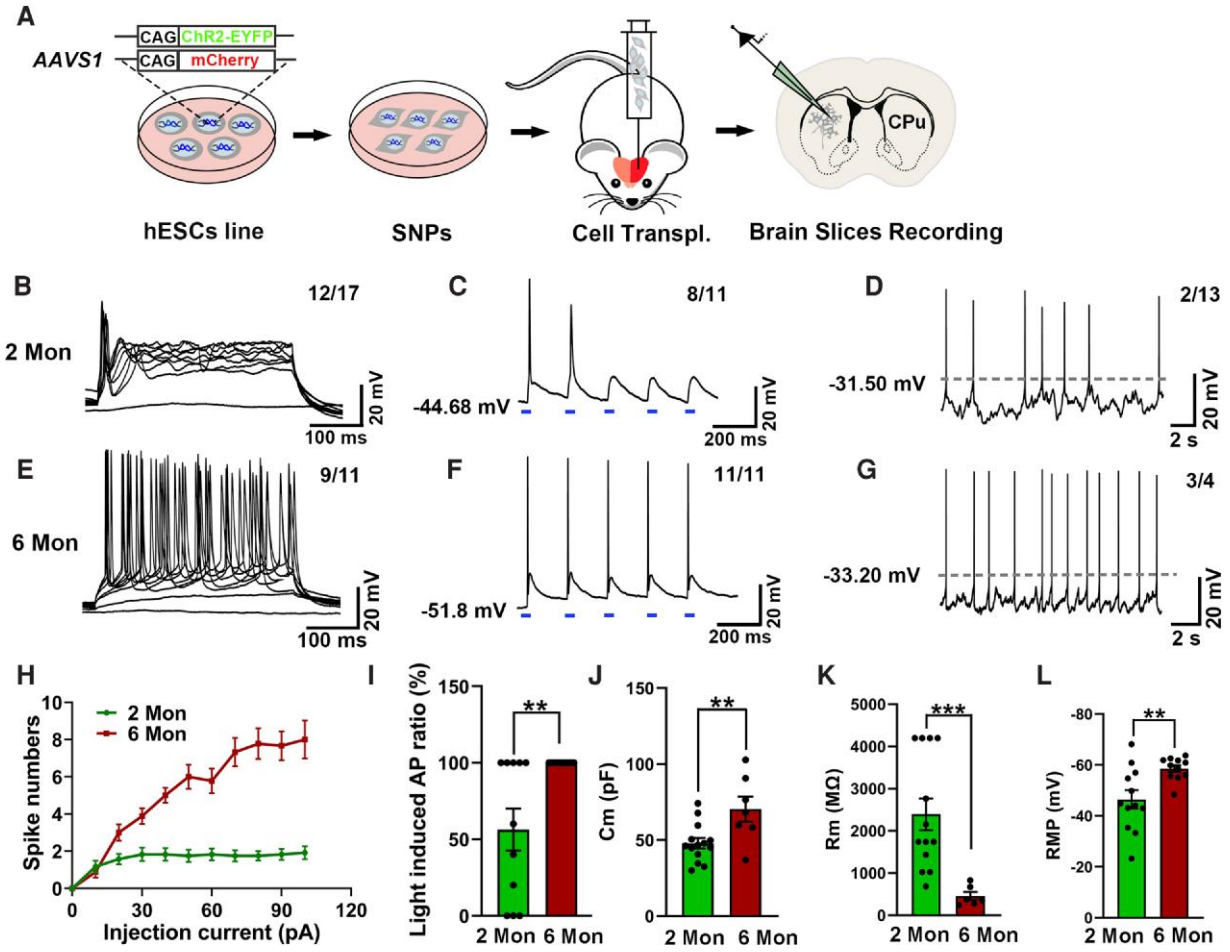

Figure 2 Neuronal activity of grafted neurons in the ipsilateral striatum of the HIE-injured brain. (**A**) The strategy for electrophysiological recording of grafted human neurons. (**B**–**G**) Typical traces of injection current- (**B** and **E**) or blue light- (**C** and **F**) induced AP and spontaneous AP (**D** and **G**) of grafted neurons 2 and 6 MPT. The numbers in the upper right corner represent the numbers of neurons showing AP among recorded cells. (**H**) The current (0–100 pA, step 10 pA, duration 400 ms) induced spike numbers of grafted neurons 2 MPT ($n = 12$) or 6 MPT ($n = 9$). (**I**) Quantification of the AP ratio showed a significantly increased response to blue light stimulation at 6 months ($n = 11$) compared to 2 months ($n = 11$) after cell transplantation. (**J**–**L**) Statistical data show increased membrane capacitance ($n = 14$ for 2 months, $n = 7$ for 6 months) (**J**), decreased membrane resistance, recorded cell number ($n = 13$ for 2 months, $n = 6$ for 6 months) (**K**) and increased resting membrane potentials ($n = 12$ for 2 months, $n = 11$ for 6 months) of grafted neurons at 6 MPT compared with 2 MPT. (**L**). $n = 3$ independent experiments. Data are presented as the mean ± SEM. Student's *t*-test, $^{**}P < 0.01$, $^{***}P < 0.001$. AP = action potential; Cm = membrane capacitance; CPu = caudate putamen; Rm = membrane resistance; RMP = resting membrane potential.

cell transplantation, AAV expressing the Cre-dependent TVA (the receptor of engineered surface protein EnvA which originates from the avian leukosis virus) with a nuclear location signal (AAV-DIO-TVA-2A-NLS-tdTomato) and AAV expressing a Cre-dependent rabies glycoprotein (G) (AAV-DIO-G) were co-injected into the graft site to express TVA and G specifically in the transplanted cells. Then, EnvA-pseudotyped and G-deleted rabies virus tagged EGFP (RVdG-EGFP) was injected into the same area 3 weeks later to infect TVA-expressing grafted neurons ($tdTomato^+$). Thus, the grafted cells coexpressing EGFP and tdTomato are the starter cells, and expression of G in these cells enables RVdG-EGFP to spread trans-synaptically to their upstream presynaptic input cells, which will express EGFP only.[36]

Representative images showed that tdTomato was expressed only in transplants of HIE-injured brains at 2 or 6 MPT, suggesting the specificity of the rabies tracing system (Fig. 5B). The starter cells were identified by coexpression of TVA-tdTomato and EnvA-GFP ($tdTomato^+/GFP^+$), and they were also positive for GABA and hN (Fig. 5C). The starter cells were only found in the injected site and could be easily distinguished from traced neurons in intratransplants or brain regions away from the graft ($tdTomato^-/EGFP^+$). Serial section immunostaining revealed monosynaptic traced $EGFP^+$ host neurons distributed in multiple areas of the HIE-injured brain as early as 2 MPT (Fig. 5D), suggesting early host-to-graft synaptic inputs in the HIE-injured brain. Immunofluorescent staining showed that grafted striatal neurons receive synaptic inputs mostly from the cortex (M2, M1, S1), which expresses CTIP2, SATB2, BRN2 and TBR1, suggesting synaptic connectivity between graft and host excitatory neurons from different cortical layers (Supplementary Fig. 4A and B). The host-to-graft synaptic inputs also come from GPe neurons expressing parvalbumin (PV), midbrain SNc neurons expressing TH, thalamus including ventral posterolateral/posteromedial thalamic nucleus (VPL/VPM), parafascicular thalamic nucleus (PF), mediodorsal thalamic nucleus (MD) and hindbrain including dorsal raphe (DR) (Fig. 5D and E and Supplementary Fig. 4A and B), indicating extensive synaptic inputs from these brain regions to grafted spiny projection neurons, which are strikingly similar to the circuits of their endogenous

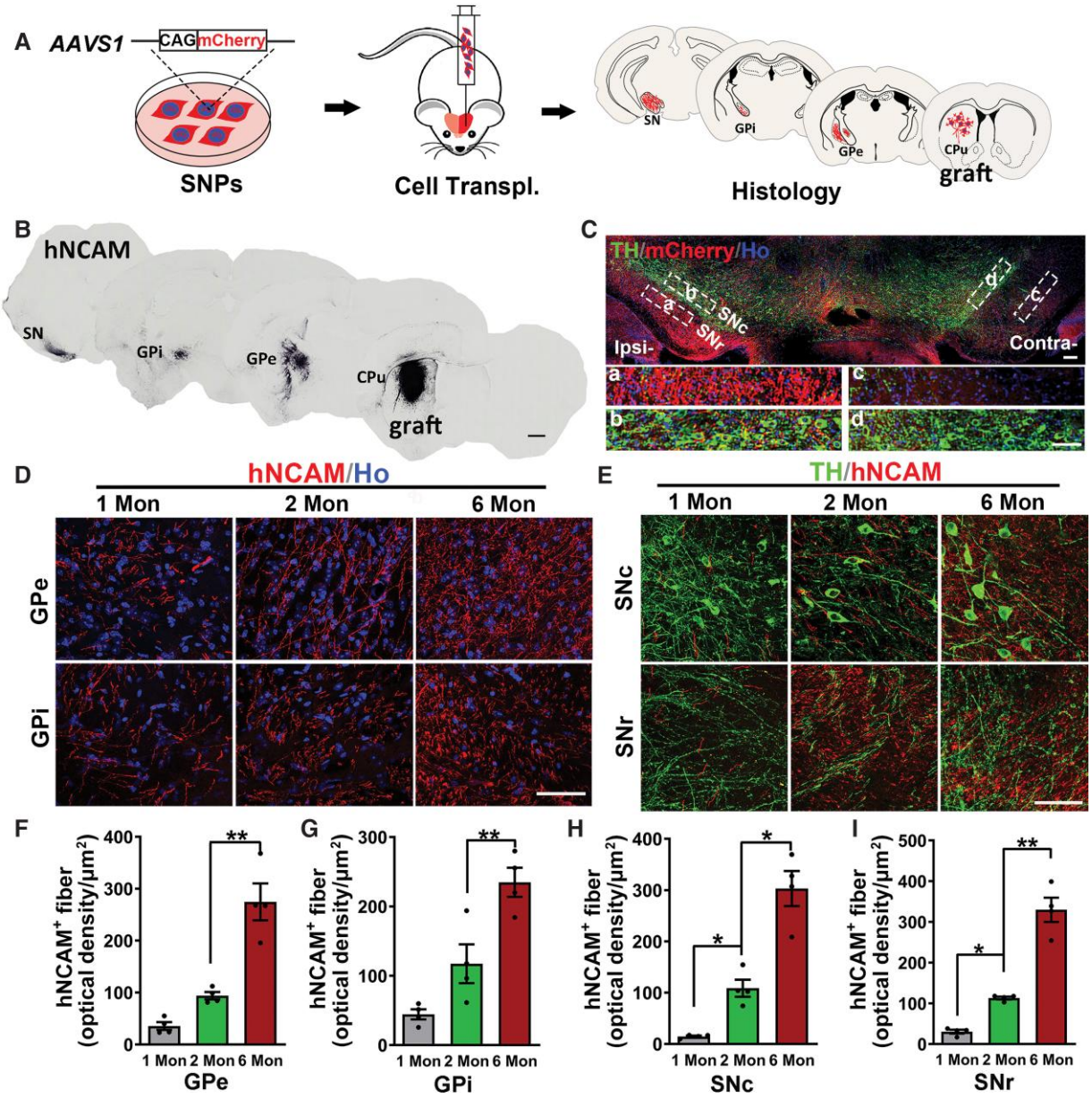

Figure 3 Axonal outgrowth of grafted striatal neurons in the HIE-injured brain. (**A**) The strategy for visualization of axon projection from grafted neurons in HIE-injured mice. (**B**) Immunohistochemical staining of hNCAM for human neurons with serial sections from HIE-injured mouse brains grafted with human SNPs 6 months after transplantation. Scale bar = 500 μm. (**C**) Representative images show axonal projections from the intrastriatal grafted neurons stained by mCherry in the ipsilateral and contralateral substantia nigra of HIE-injured mouse brains. Boxed areas are magnified in **a**–**d**. Scale bar = 50 μm. (**D** and **E**) Immunostaining of hNCAM shows axons from grafted neurons to the GPe, GPi, SNc and SNr of HIE-injured brain at 1, 2 and 6 after cell transplantation. Scale bar = 50 μm. (**F**–**I**) Quantification of hNCAM$^+$ fibres present in GPe, GPi, SNc and SNr. $n = 4$ mice in each group. Data are represented as the mean ± SEM. One-way ANOVA, Tukey's multiple comparison test, $^*P < 0.05$, $^{**}P < 0.01$.

counterpart.[37] To investigate how the map of host-to-graft synaptic inputs would change at a longer time after cell transplantation, we further detected synaptic inputs from host to graft 6 MPT. Interestingly, we found that the distribution and proportion of GFP-labelled neurons in most brain regions were similar except in the VPL/VPM and DR between 2 and 6 MPT (Fig. 5E), suggesting extensive and stable host-to-graft synaptic connections at very early stage after human SNP transplantation in HIE-injured brains. Together, these data strongly suggest precise re-establishment of anatomical basal ganglia neural circuits by hESC-derived SNPs in HIE-injured brains.

Grafted neurons receive synaptic regulation from the striatal and cortical neurons of the HIE-injured brain

To investigate whether the grafted neurons could functionally integrate into the host neural circuitry, SNPs derived from hESC-mCherry were transplanted into the ipsilateral striatum of the HIE-injured brain, and sIPSCs or sEPSCs of the transplanted cells were recorded by patch clamp electrophysiology at 2 and 6 MPT, respectively (Fig. 6A). A total of 100% (8/8) of grafted neurons showed abundant sIPSCs or sEPSCs with high density by 6 MPT (Fig. 6C), while only 50% (9/18) were recorded with few sIPSCs or

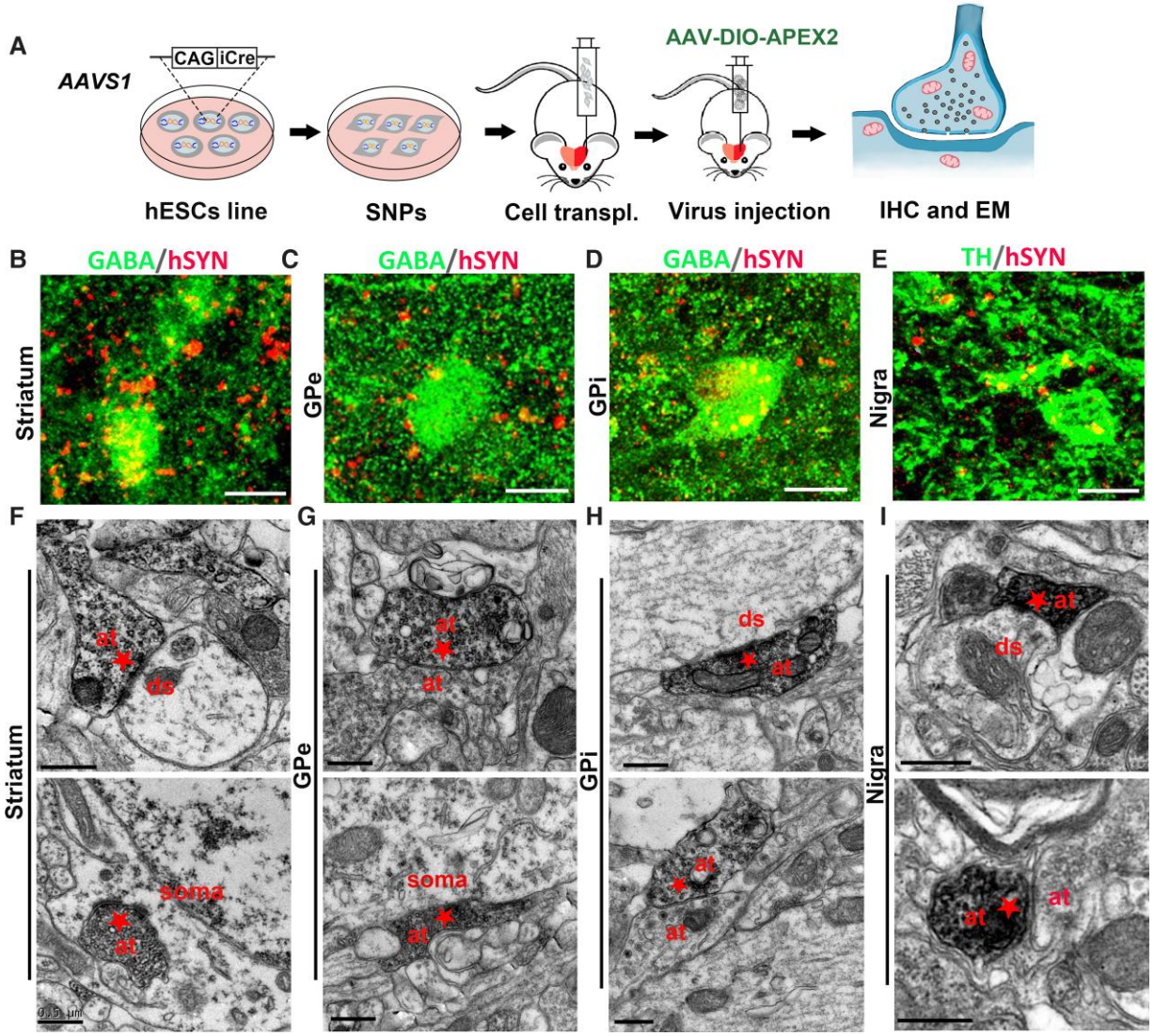

Figure 4 Synapse formation between grafts and hosts in HIE-injured brains. (**A**) The strategy for Cre-dependent visualization of synapses between host and graft. (**B–E**) Representative images show presynaptic human synaptophysin costained with host GABA$^+$ neurons in the striatum (**B**), GPe (**C**), GPi (**D**) or with host TH$^+$ neurons in the substantia nigra (**E**) of HIE-injured brains. Scale bar = 10 μm. (**F–I**) Representative images of immunoelectron microscopy show axon terminals (at) from grafted neurons (asterisks) form synapses with dendrite spines (ds), soma or axon terminals from host neurons in the striatum (**F**), GPe (**G**), GPi (**H**) and the substantia nigra (**I**). Scale bar = 0.5 μm.

sEPSCs by 2 MPT (Fig. 6B), suggesting gradual integration of grafted cells into neural networks in the HIE-injured brain. The statistical data showed dramatically increased frequencies of sEPSCs ($P < 0.05$; Fig. 6D) and sIPSCs (Fig. 6F) at 6 MPT (1.99 ± 0.58 Hz for sEPSCs; 4.85 ± 1.47 Hz for sIPSCs) compared to 2 MPT (0.51 ± 0.29 Hz for sEPSCs; 0.62 ± 0.43 Hz for sIPSCs). Plotting of a cumulative distribution of sEPSCs and sIPSC intervals is shown in Fig. 6H and J. Interestingly, the amplitude of sIPSCs significantly increased ($P < 0.01$) at 6 MPT (19.36 ± 1.70 pA) in contrast to 2 MPT (12.43 ± 0.93 pA; Fig. 6G), while the sEPSCs showed no changes between these two groups (Fig. 6E). However, the cumulative fraction of sIPSCs and sEPSCs both showed an obviously higher amplitude at 6 than at 2 MPT (Fig. 6I and K). The recorded human neurons were confirmed by biocytin, which was co-labelled with mCherry (Supplementary Fig. 5A). No significant differences in the half-width, rise time or decay time of sEPSCs or sIPSCs were observed at 2 and 6 MPT (Supplementary Fig. 5C–H).

To further explore whether the activities of transplanted cells could be regulated by host cortical neurons, we injected an AAV virus expressing ChR2 fused with EYFP under the control of the human synapsin promoter into the motor cortex (M1 and M2) at 5 MPT (Fig. 6A). One month later, many ChR2-EYFP-expressing axon terminals from the cortical M1 and M2 regions were observed around the intrastriatal grafted cells (Supplementary Fig. 5B). After blue light stimulus, approximately 83% of transplanted cells (10/12) were recorded with induced EPSC, which was completely blocked by the AMPA receptor antagonist CNQX, indicating glutamatergic presynaptic inputs from host to graft (Fig. 6L). The amplitude of EPSC is shown in Fig. 6M. The electrophysiological recorded cell was costained by biocytin and mCherry surrounded by many EGFP$^+$ axons, confirming grafted human neurons in the striatum and axon projections from cortical ChR2-expressing host neurons (Supplementary Fig. 5B). Furthermore, the paired pulse ratio (PPR), which is the ratio of the amplitude of the second response to that of

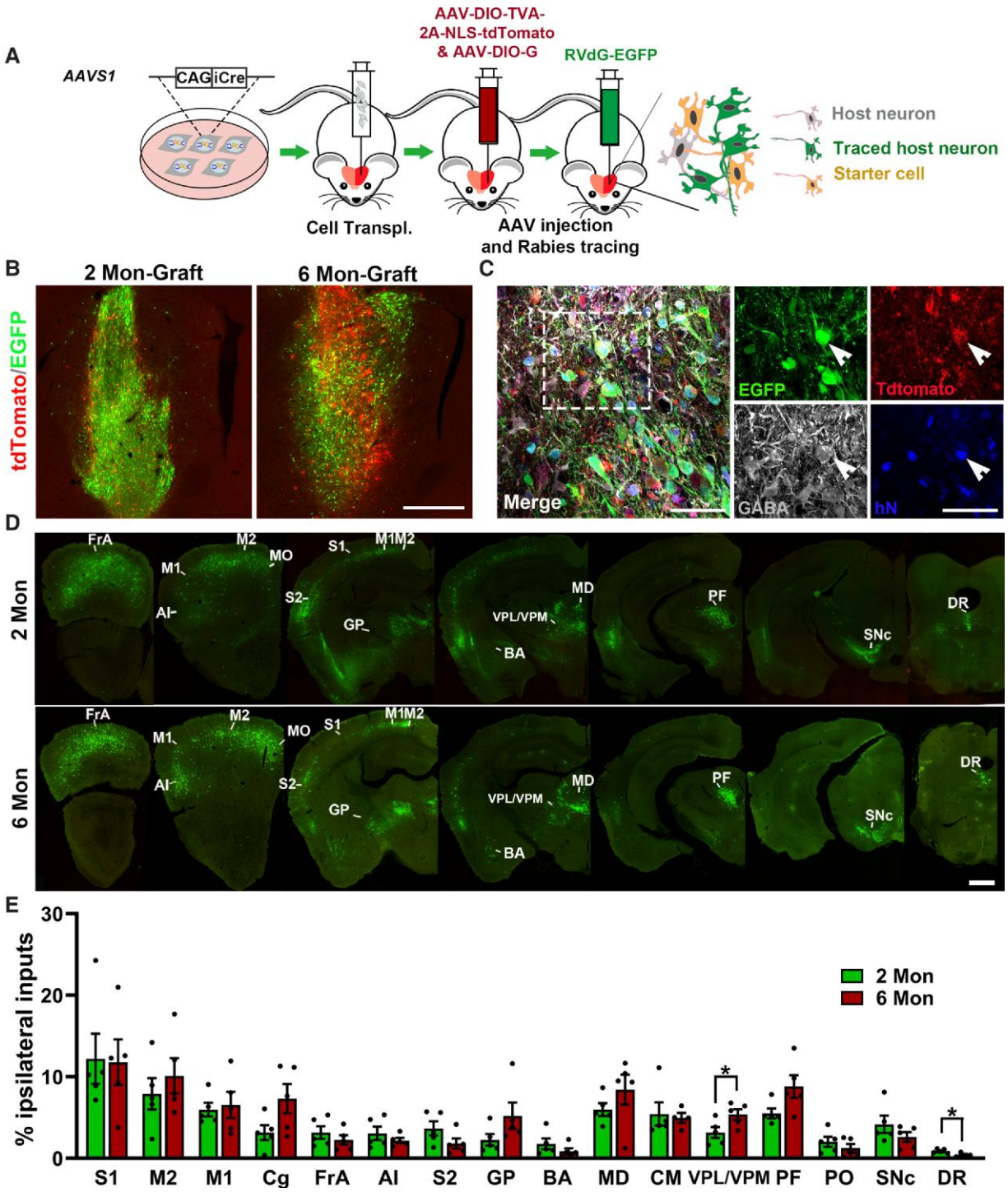

Figure 5 Synaptic inputs from host to graft by rabies tracing in HIE-injured brain. (**A**) Strategy for tracing synaptic inputs to grafted cells in the ipsilateral striatum of the HIE-injured brain. (**B**) Representative images show EGFP- and tdTomato-expressing neurons in the grafts. Scale bar = 500 μm. (**C**) Immunohistochemical staining show the starting cells (arrowheads) coexpress tdTomato, EGFP, GABA and hN in the graft. Scale bar = 50 μm. (**D**) Serial sections from HIE-injured brain grafted with SNPs show traced host neurons ($EGFP^+/tdTomato^-$) distribute in extensive brain regions of the ipsilateral side 2 and 6 MPT. Scale bar = 500 μm. (**E**) Quantification of ipsilaterally labelled inputs to grafted human SNPs at 2 and 6 MPT. $n = 4$–5 mice in each group. Data are presented as the mean ± SEM. Student's *t*-test, $^*P < 0.05$. AI = agranular insular cortex; BA = basal amygdaloid nucleus; Cg = cingulate cortex; CM = central medial thalamic nucleus; DR = dorsal raphe; GP = globus pallidus; FrA = frontal association cortex; M1 = primary motor cortex; M2 = secondary motor cortex; MD = mediodorsal thalamic nucleus; MO = medial orbital cortex; PF = parafascicular thalamic nucleus; PO = posterior thalamic nucleus; S1 = primary somatosensory cortex; S2 = secondary somatosensory cortex; SNc = substantia nigra reticular part; VPL/VPM = ventral posterolateral/posteromedial thalamic nucleus.

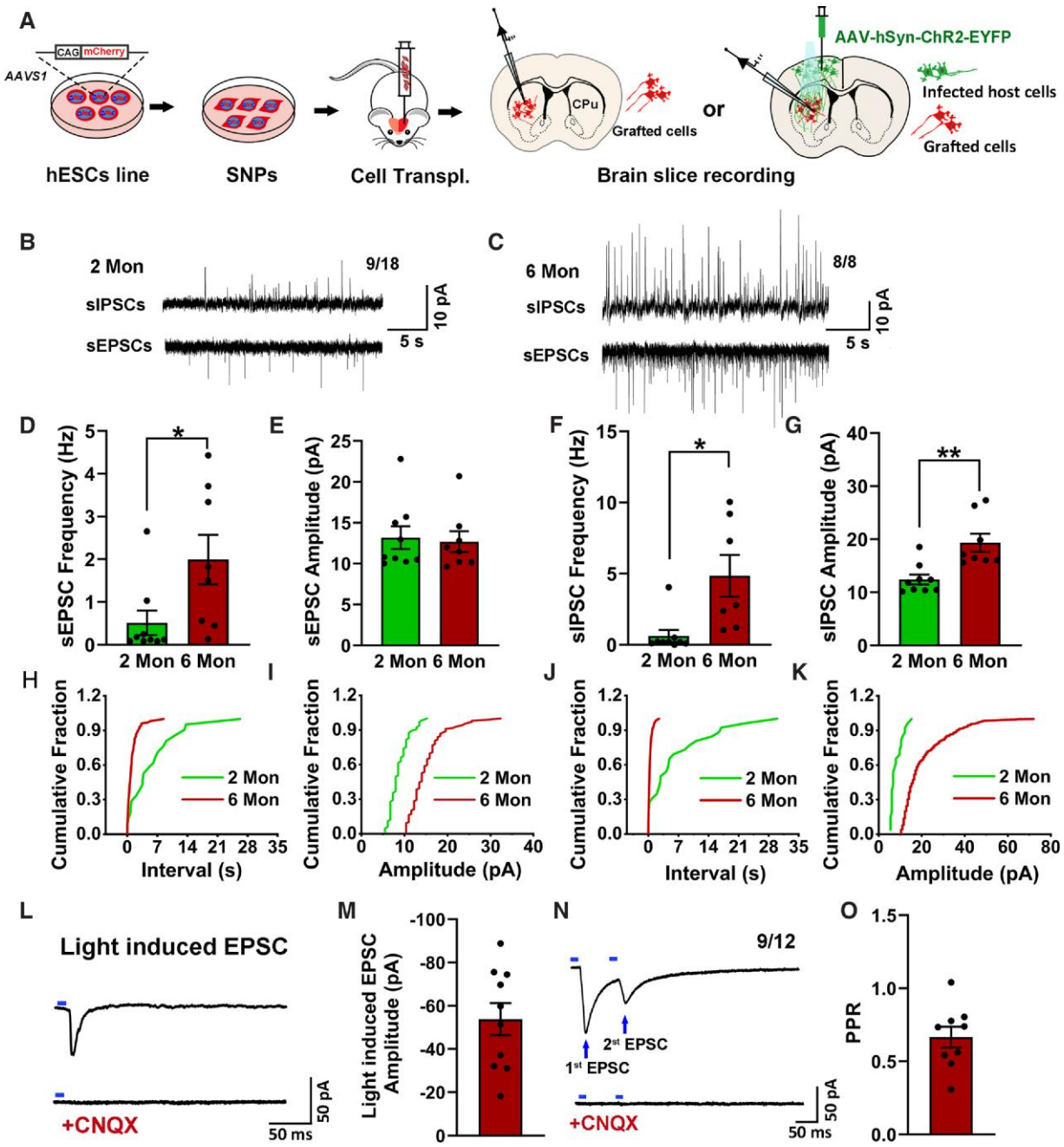

Figure 6 Synaptic regulation of grafted striatal neurons in the HIE-injured brain. (**A**) The strategy for whole-cell patch-clamp recording of synaptic regulation from the host striatum or cortex to intrastriatally grafted striatal neurons. (**B** and **C**) Typical traces of sEPSCs and sIPSCs from grafted neurons at 2 and 6 MPT. The numbers in the upper right corner represent the numbers of neurons showing spikes of sIPSCs and sEPSCs among recorded cells. (**D**–**G**) The frequency (**D** and **F**) and amplitude (**E** and **G**) of sEPSCs and sIPSCs at 2 ($n = 9$ for sEPSCs, $n = 9$ for sIPSCs) and 6 MPT ($n = 7$ for sIPSCs, $n = 8$ for sEPSCs) are plotted. (**H**–**K**) Cumulative distributions of the interevent intervals (**H** and **J**) and amplitude (**I** and **K**) of sEPSCs and sIPSCs for (**B**) and (**C**), respectively. (**L** and **M**) Typical traces of single pulse-induced EPSCs in grafted cells responding to optogenetic activation of host cortical neurons from M1 and M2 brain regions 6 MPT (*top*), which are blocked by CNQX (*bottom*). The amplitude of light-induced EPSC is plotted in (**M**) ($n = 10$). (**N**) Typical traces of paired pulse-induced EPSCs in grafted cells responding to optogenetic activation of host cortical neurons in M1 and M2 at 6 MPT (*top*), which are blocked by CNQX (*bottom*). (**O**) The paired pulse ratio (PPR = 2nd EPSC/1st EPSC) is plotted ($n = 9$). Data are presented as the mean ± SEM, $^{*}P < 0.05$, $^{**}P < 0.01$.

the first, was also tested in grafted neurons upon light stimulation. By giving a paired pulse of two consecutive stimulations, 75% of the grafted cells (9/12) were recorded with PPR (Fig. 6N, top). The second peak amplitude is smaller than that of the first (Fig. 6N, top) which the PPR is 0.67 ± 0.07 (Fig. 6O), suggesting established plasticity of grafted neurons in the HIE-injured brain. The paired pulse disappeared after CNQX treatment, suggesting an AMPA receptor-dependent postsynaptic response of grafted neurons (Fig. 6N, bottom).

Together, these results indicate functional integration of intrastriatal grafted neurons into striatal and corticostriatal neural circuits in the HIE-injured brain.

Intrastriatal grafted neurons activate host striatal and long-range targeted nigra neurons in HIE-injured brains

To test whether the grafted neurons could regulate the activity of host neurons, we transplanted SNPs derived from the hESC-ChR2-EYFP line into the ipsilateral striatum of HIE mice and recorded the response of the host neurons to blue light stimulus on the grafted neurons at 2 and 6 MPT. First, we performed whole-cell patch-clamp recordings on host striatal neurons at 2 and 6 MPT (Fig. 7A–C). The statistical data showed that approximately 83% of host neurons (15/18) showed light-induced IPSC with 64.35 ± 17.11 pA amplitude at 2 MPT (Fig. 7B and G), which then significantly increased to 135.30 ± 24.80 pA with 100% (13/13) responses of host neurons to graft cells by 6 MPT (Fig. 7C and G), indicating progressive establishment of intrastriatal neural networks and successful graft-to-host synaptic regulation in the ipsilateral striatum of the HIE-injured brain. The recorded host cells were stained by biocytin but not EGFP, suggesting host neurons of the striatum (Supplementary Fig. 6E). In addition, the blue light-induced IPSC was completely blocked by the GABAR antagonist PTX, indicating GABAergic presynaptic currents from the graft (Fig. 7B and C, bottom). Striatal GABA neurons derived from the hESC-mCherry line were used as the control for optogenetic activation of grafted cells in the striatum of HIE-injured mice (Supplementary Fig. 6A), which showed properties of mature neurons but no APs evoked by blue light illumination at 6 MPT (Supplementary Fig. 6B–D).

Notably, we also investigated evoked IPSCs of host dopaminergic neurons in the SNc, the long-range targeted host neurons of the intrastriatal transplanted spiny projection neurons. By blue light stimulation of ChR2-EYFP-expressing axon terminals (Fig. 7D), we found obvious light-induced IPSCs as early as 2 MPT, although the amplitude was relatively low (20.23 ± 3.69 pA; Fig. 7E and H), suggesting early formed axon projections and appropriate synaptic outputs from the striatal graft to their targeted host neurons. Then, the amplitude significantly increased to 81.16 ± 14.41 pA by 6 MPT ($P < 0.01$; Fig. 7F and H), indicating functional integration of grafted neurons into the striatal–nigra neural circuit of the HIE-injured brain. In the SNc, we can see obvious EGFP-positive fibres that projected from striatal grafted human neurons dispersed around the recorded dopaminergic neurons stained by biocytin and TH (Supplementary Fig. 6F).

Taken together, these data strongly suggested that transplanted human striatal neurons establish functional intrastriatal and striatal–nigra neural circuits in HIE-injured brains.

Transplanted hESC-derived striatal neurons correct the motor deficits of HIE-injured mice in the long term

In HIE-injured patients, the impairment of the basal ganglia neural circuit is mostly associated with motor deficits.[15] To further investigate whether hESC-derived SNPs could rescue the motor behaviours of animals with HIE injury in the long term, we transplanted the ipsilateral striatum of HIE mice with hESC-derived SNPs or spinal GABA neural progenitors (SGNPs), which will differentiate into spinal GABA interneurons,[31] as control cells. In addition, we also used HIE-injured mice transplanted with ACSF and sham (surgery without artery ligation and hypoxia) animals as control of cell therapy and HIE mouse models, respectively. Then, animals were subjected to motor activity-related behavioural tests, including cylinder, open field and rotarod tests, at 2, 4 and 6 MPT to determine whether the motor behavioural defects were corrected in each group (Fig. 8A). In the cylinder test, which reflects forelimb akinesia, HIE mice grafted with SNPs (***$P < 0.001$) significantly reduced preferential ipsilateral touches to nearly 50% (the level in sham animals) as early as 2 MPT until 6 MPT but not for animals that received SGNPs or ACSF (Fig. 8B). For the open field test, which reveals limb movements during locomotion, the total distance covered by HIE-injured mice was significantly increased over time by intrastriatal SNPs transplantation ($P < 0.001$) but not by SGNPs or ACSF treatment (Fig. 8C). In addition, motor coordination and balance assessed by the rotarod test also exhibited obviously increased latency on the rotarod in HIE-injured animals grafted with SNPs but not SGNPs or ACSF (Fig. 8D). Representative images showed a large number of human cells (hN^+) stained by GABA but not DARPP32 distributed in the ipsilateral striatum of HIE-injured mice at 6 MPT (Supplementary Fig. 7A and B), indicating maturation of hESC-derived spinal GABA neurons in host striatum. Few cell bodies but not neuron fibres were present in the SNc and SNr of the SN, suggesting migration of the grafted spinal GABA neurons from the striatum (Supplementary Fig. 7C and D).

To determine whether the improved motor function of HIE-injured mice was graft-dependent, we transplanted SNPs derived from hESCs-hM4Di-mCherry, an engineering inhibitory DREADD,[38] or hESCs-mCherry as a control into the ipsilateral striatum of HIE-injured mice (Fig. 8E). The statistical data of the cylinder test showed that CNO but not saline treatment significantly increased the preferential ipsilateral touches of mice grafted with hM4Di-SNPs ($P < 0.01$), which then returned to the control level 48 h after CNO withdrawal ($P < 0.05$), suggesting graft activity-dependent behavioural changes in HIE-injured mice. CNO treatment had no effect on ipsilateral touches in mice that received SNPs expressing mCherry (Fig. 8F). In the open field test, CNO treatment significantly decreased the total distance covered by mice grafted with hM4Di-SNPs compared to saline treatment or CNO withdrawal ($P < 0.05$), but not in animals grafted with Cherry-SNPs (Fig. 8G), indicating graft-dependent improvement of animal motor functions. Together, these data strongly indicated that motor deficits in HIE-injured mice could be rescued in the long term by intrastriatal transplantation of spiny projection neurons but not spinal GABA neurons and graft-dependent behavioural recovery in HIE-injured animals.

Discussion

Here, we showed hESC-derived SNPs survived and matured into striatal spiny projection neurons in HIE-injured brains, and we first proved the high feasibility and long-term therapeutic efficiency of hESC-derived striatal neural progenitors in immature HIE-injured brains, including neuronal survival and differentiation, axon projections and synapse formation, neural circuit reconstruction and functional restoration.

Currently, hypothermia treatment is the only clinically established intervention following neonatal HIE. However, almost half of all cooled infants still die or suffer from long-lasting neurological impairments because of the short time window (within 6 h) and limited effects, particularly in some severe cases.[1,39] Transplantation of neural progenitor cells or neural stem cells to treat HIE has been much explored, and while most of them focused on the therapeutic effects of transplanted cells in short term in HIE mice, the underlying mechanisms have been poorly investigated. Some studies showed that transplanted neural progenitors can

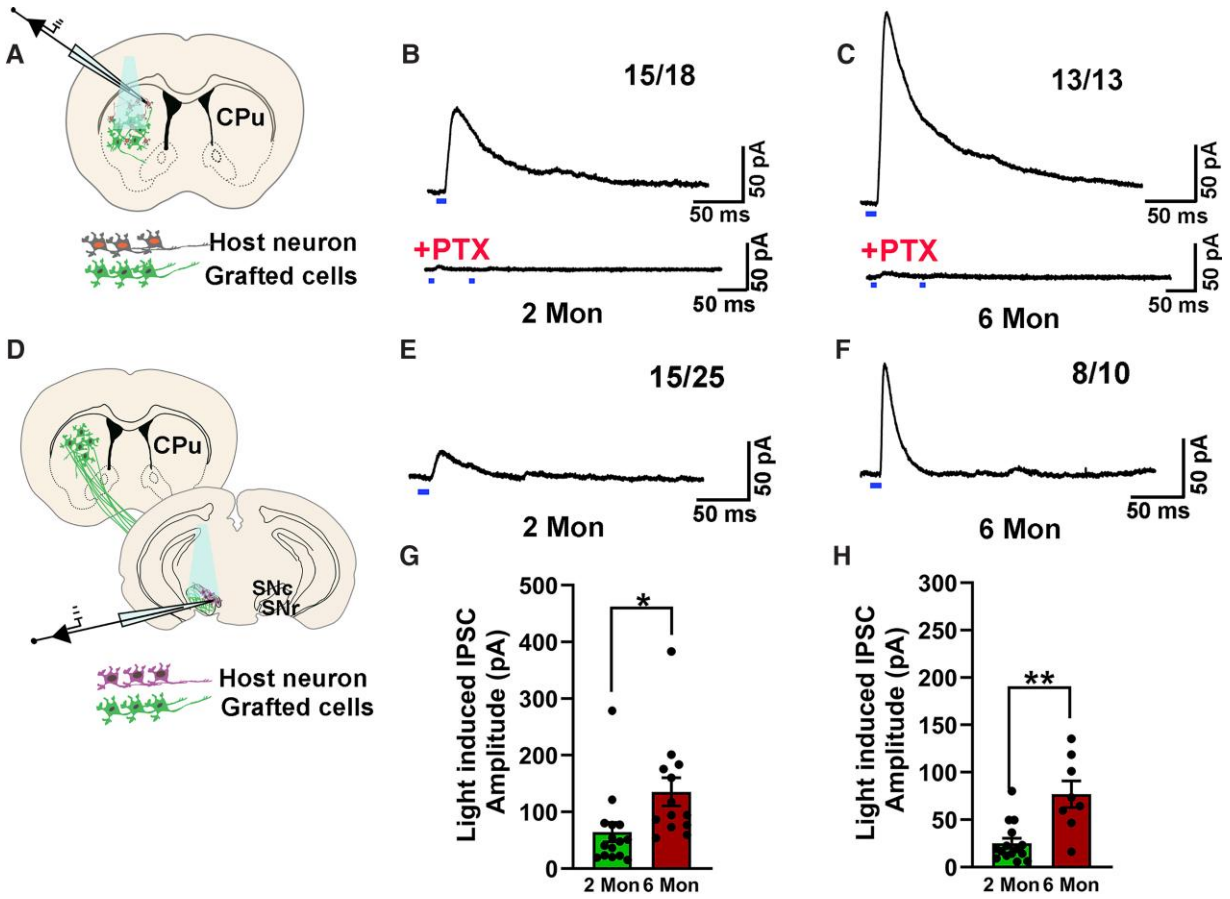

Figure 7 Grafted striatal neurons regulate the activities of host neurons from the striatum and nigra of HIE-injured brains. (**A**) Schematic diagram showing the whole-cell patch-clamp recording of host striatal neurons. (**B** and **C**) Typical traces of blue light-induced IPSC of striatal host cells responding to optogenetic activation of grafted cells at 2 months (**B**) and 6 months (**C**) after transplantation. The induced IPSC is blocked by PTX (*bottom*). (**D**) Schematic diagram showing the whole-cell patch-clamp recording of host cells in the SNc. (**E** and **F**) Typical traces of blue light-induced IPSCs in nigral host cells responding to optogenetic activation of axonal terminals from grafted neurons at 2 months (**E**) and 6 months (**F**) after transplantation. (**G** and **H**) The amplitude of light-induced IPSC in the striatal (**G**) ($n = 15$ for 2 months, $n = 13$ for 6 months) or nigra (**H**) ($n = 15$ for 2 months, $n = 8$ for 6 months) host neurons are plotted. Data are presented as the mean ± SEM. Student's *t*-test, $^{*}P < 0.05$, $^{**}P < 0.01$.

secrete multiple factors, modify microglial response[40] or enhance axonal sprouting of host neurons. However, the causal roles of these effects in the functional recovery of HIE model animals have not been demonstrated. In the current study, we showed that transplanted striatal progenitor cells can specifically project to their cognate brain regions including GPe, GPi and SN (Fig. 3) and receive innervation from host neurons in multiple brain areas (Fig. 5) in a pattern similar to their endogenous counterparts.[37] We further demonstrated that transplanted striatal neurons can form functional synaptic connection with host neurons both pre- and postsynaptically (Figs 6 and 7). Finally, by modulating graft activity with chemogenetic tools, we demonstrated that the functional recovery of HIE model mice depends on the graft activity. These results explicitly suggest that transplanted striatal spiny projection neurons can reconstruct specific circuits that account for the functional recovery of HIE model animals.

Previously, donor cells with unclear regional identity or fate potentials were used,[2,41–43] meaning the therapeutic outcomes varied among different studies. Some transplanted cells even containing undifferentiated ESCs or immature ectoderm,[44] which probably explains why model animals injected with these donor cells developed local tumors.[41] In the current study, we used fate-committed striatal GABA neural progenitors without any embryonic stem cell markers (Supplementary Fig. 2A), which can efficiently differentiate into DAPP32^{+} striatal GABA projection neurons (90%) *in vitro* or after transplantation *in vivo* (Fig. 1). We also showed that transplantation of striatal GABA neural progenitors but not spinal GABA neural progenitors can specifically project and rescue the motor deficits of HIE-injured mice in the long term (Fig. 8). These results suggest that the identity of transplanted neuronal cells determines their axonal projection specificity and functionality. We hypothesize that transplantation of fate-committed neural progenitor cells with proper identity is essential for reconstructing certain damaged circuits with specificity.

Although stem cell-based replacement therapy shows great potential by neural circuit reconstruction in adult disease models such as Parkinson's disease[25] and Huntington's disease,[24] it has rarely been studied in immature brain with HIE injury before. Here, we found that striatal grafted SNPs send axons as early as 1 month to endogenous target areas after cell transplantation in HIE-injured brains, similar to the SNPs grafted in adult Huntington's disease mouse brains,[24] indicating intrinsic cell properties probably determine the targeted projection of grafted human neurons.[25,45] After axon extension, grafted neurons should form synaptic connections with host neurons. In HIE-injured brains, the grafted SNPs receive synaptic inputs from extensive brain

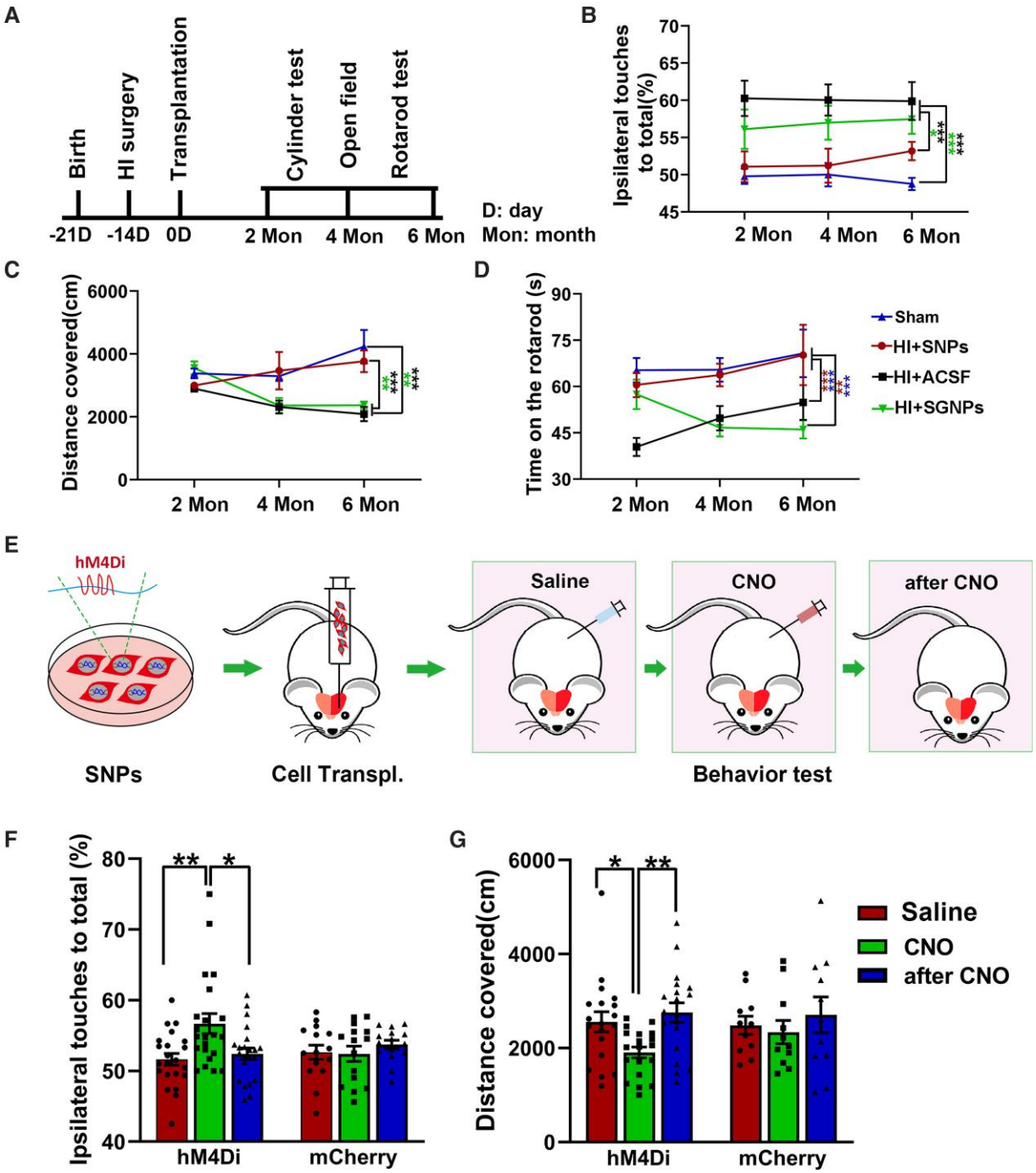

Figure 8 Intrastriatally grafted SNPs correct long-term and graft-dependent motor defects in HIE-injured mice. (**A**) Experimental design for animal behavioural tests. (**B**) The cylinder test shows the preferential ipsilateral touches in sham control, HIE-injured mice grafted with SNPs or spinal GABAergic neural progenitors (SGNPs) or ACSF at 2, 4 and 6 MPT. (**C**) The open-field test shows distance covered by animals in each group at 2, 4 and 6 MPT. (**D**) The rotarod test shows the time of latency to fall over 6 MPT. In above behavioural tests, $n = 12–17$ for the sham group, $n = 10–15$ for the HI + SNPs group, $n = 10–15$ for the HI + ACSF group and $n = 7–11$ for the HI + SGNPs group. Data are presented as the mean ± SEM. Two-way ANOVA followed by Tukey's multiple comparison test, $^{*}P < 0.05$, $^{**}P < 0.01$, $^{***}P < 0.001$. (**E**) The strategy for the regulation of DREADD-expressing grafted neurons in HIE-injured mice 6 MPT. (**F**) The cylinder test shows changes in preferential ipsilateral touches of HIE-injured mice grafted with SNPs derived from hM4Di- or mCherry-hESC lines and treated with saline or CNO or 48 h after withdrawal of CNO, respectively. (**G**) The open-field test shows changes in the distance covered by HIE-injured mice treated with saline, CNO or 48 h after CNO withdrawal, respectively. $n = 9–13$ mice in each group. Data are presented as the mean ± SEM. One-way ANOVA followed by Tukey's multiple comparison test, $^{*}P < 0.05$, $^{**}P < 0.01$.

regions, similar to their endogenous counterparts,[37] by 2 MPT. However, only cell transplantation sites where the synaptic inputs stem from the grafted neurons were observed in Huntington's disease model mice.[24] As similar human neural progenitors were transplanted, these results suggest that extrinsic but not intrinsic cell determinants affect the formation of synaptic connections

between grafted human neurons and host neurons. However, what exactly determines neural circuit restoration in the injured brain still needs to be explored. Many previous studies have shown that the initial growth and guidance of axons are mostly regulated by genetically predetermined programmes, while the late steps of synapse and neuronal connectivity formation and neural circuit integration are influenced by neurotrophin and neuron-glia activation during brain development,[46,47] which indicates that different microenvironments of the host brain may affect formation of synaptic connection during neural circuit regeneration in diseased brains. Intriguingly, we found that brain regions of the afferent synaptic inputs to the graft did not differ between 2 and 6 MPT, indicating that stable synaptic connections formed at 2 MPT. However, these newly formed synaptic connections do not functionally mature, as revealed by significantly lower host-to-graft sEPSCs and sIPSCs at 2 than at 6 MPT, suggesting sequential but not synchronous establishment of synaptic connections between transplanted human neurons and host cells in the HIE-injured brain.

In the current study, we mainly tested and proved proof-of-principle for the treatment of neonatal HIE by grafting hESC-derived striatal neurons in a HIE mouse model. From a clinical perspective, hESCs and their differentiated derivatives express low levels of HLA molecules,[48,49] the major determinant of immunogenicity in stem cell therapy, suggesting probably minor immune response after cell transplantation *in vivo*. Besides, hESC-derived neural progenitors have been approved for clinical trials in the USA and China.[50,51] These studies suggest hESC-derived SNPs could be a proper cell type for stem cell therapy of HIE. However, the use of hESCs may confront potential ethical issues in some countries, and personalized iPSC-derived neural progenitors have been proved effective in the treatment of some neurological diseases without detectable immune rejection in clinical studies of human participants.[52,53] Further investigation about therapeutic effects of striatal neural progenitors derived from iPSCs in the treatment of HIE need to be done in the future.

Funding

This study was supported in part by the National Key Research and Development Program of China (2018YFA0108000); the Strategic Priority Research Program of the Chinese Academy of Sciences (XDB32010100); National Natural Science Foundation of China (82222021, 32270849, 82130048, 81974174, 81720108018, 32170806); Shanghai Municipal Science and Technology Major Project (2018SHZDZX05, 2018SHZDZX01), ZJ Lab and Shanghai Center for Brain Science and Brain-Inspired Technology; Major Research Projects for Young and Middle-aged People of Fujian Province (2021ZQNZD017); State Key Laboratory of Neuroscience (SKLN-201704); National Science and Technology Innovation 2030 Major Program (2021ZD0200900); Program of Shanghai Academic/Technology Research leader (22XD1420800).

Competing interests

The authors declare no competing interests.

Supplementary material

Supplementary material is available at *Brain* online.

References

1. Douglas-Escobar M, Weiss MD. Hypoxic–ischemic encephalopathy: A review for the clinician. *JAMA Pediatr*. 2015;169:397-403.
2. Lee BL, Glass HC. Cognitive outcomes in late childhood and adolescence of neonatal hypoxic–ischemic encephalopathy. *Clin Exp Pediatr*. 2021;64:608-618.
3. Azzopardi D, Strohm B, Marlow N, *et al*. Effects of hypothermia for perinatal asphyxia on childhood outcomes. *N Engl J Med*. 2014;371:140-149.
4. Perez A, Ritter S, Brotschi B, *et al*. Long-term neurodevelopmental outcome with hypoxic–ischemic encephalopathy. *J Pediatr*. 2013;163:454-459.e1.
5. Ahn SY, Chang YS, Park WS. Stem cells for neonatal brain disorders. *Neonatology*. 2016;109:377-383.
6. Huang L, Zhang L. Neural stem cell therapies and hypoxic–ischemic brain injury. *Prog Neurobiol*. 2019;173:1-17.
7. Nair S, Rocha-Ferreira E, Fleiss B, *et al*. Neuroprotection offered by mesenchymal stem cells in perinatal brain injury: Role of mitochondria, inflammation, and reactive oxygen species. *J Neurochem*. 2021;158:59-73.
8. Peng X, Song J, Li B, Zhu C, Wang X. Umbilical cord blood stem cell therapy in premature brain injury: Opportunities and challenges. *J Neurosci Res*. 2020;98:815-825.
9. Suzuki T, Sato Y, Kushida Y, *et al*. Intravenously delivered multilineage-differentiating stress enduring cells dampen excessive glutamate metabolism and microglial activation in experimental perinatal hypoxic ischemic encephalopathy. *J Cereb Blood Flow Metab*. 2021;41:1707-1720.
10. Park YJ, Borlongan CV, Dezawa M. Cell-based treatment for perinatal hypoxic–ischemic encephalopathy. *Brain Circ*. 2021;7:13-17.
11. Zhao M, Zhu P, Fujino M, *et al*. Oxidative stress in hypoxic–ischemic encephalopathy: Molecular mechanisms and therapeutic strategies. *Int J Mol Sci*. 2016;17:2078.
12. Rodriguez J, Li T, Xu Y, Sun Y, Zhu C. Role of apoptosis-inducing factor in perinatal hypoxic–ischemic brain injury. *Neural Regen Res*. 2021;16:205-213.
13. Rocha-Ferreira E, Hristova M. Plasticity in the neonatal brain following hypoxic–ischaemic injury. *Neural Plast*. 2016;2016:4901014.
14. Harteman JC, Nikkels PG, Benders MJ, Kwee A, Groenendaal F, de Vries LS. Placental pathology in full-term infants with hypoxic–ischemic neonatal encephalopathy and association with magnetic resonance imaging pattern of brain injury. *J Pediatr*. 2013;163:968-995.e2.
15. Martinez-Biarge M, Diez-Sebastian J, Kapellou O, *et al*. Predicting motor outcome and death in term hypoxic–ischemic encephalopathy. *Neurology*. 2011;76:2055-2061.
16. Chang PD, Chow DS, Alber A, Lin YK, Youn YA. Predictive values of location and volumetric MRI injury patterns for neurodevelopmental outcomes in hypoxic–ischemic encephalopathy neonates. *Brain Sci*. 2020;10:991.
17. Mallard EC, Waldvogel HJ, Williams CE, Faull RL, Gluckman PD. Repeated asphyxia causes loss of striatal projection neurons in the fetal sheep brain. *Neuroscience*. 1995;65:827-836.
18. Pisani A, Bonsi P, Calabresi P. Calcium signaling and neuronal vulnerability to ischemia in the striatum. *Cell Calcium*. 2004;36:277-284.
19. Tornero D, Wattananit S, Gronning Madsen M, *et al*. Human induced pluripotent stem cell-derived cortical neurons integrate in stroke-injured cortex and improve functional recovery. *Brain*. 2013;136(Pt):3561-3577.
20. Ma L, Hu B, Liu Y, *et al*. Human embryonic stem cell-derived GABA neurons correct locomotion deficits in quinolinic acid-lesioned mice. *Cell Stem Cell*. 2012;10:455-464.

21. Wu M, Zhang D, Bi C, *et al*. A chemical recipe for generation of clinical-grade striatal neurons from hESCs. *Stem Cell Rep*. 2018; 11:635-650.
22. Tornero D, Tsupykov O, Granmo M, *et al*. Synaptic inputs from stroke-injured brain to grafted human stem cell-derived neurons activated by sensory stimuli. *Brain*. 2017;140:692-706.
23. Palma-Tortosa S, Tornero D, Grønning Hansen M, *et al*. Activity in grafted human iPS cell-derived cortical neurons integrated in stroke-injured rat brain regulates motor behavior. *Proc Natl Acad Sci U S A*. 2020; 117:9094-9100.
24. Besusso D, Schellino R, Boido M, *et al*. Stem cell-derived human striatal progenitors innervate striatal targets and alleviate sensorimotor deficit in a rat model of Huntington disease. *Stem Cell Rep*. 2020;14:876-891.
25. Xiong M, Tao Y, Gao Q, *et al*. Human stem cell-derived neurons repair circuits and restore neural function. *Cell Stem Cell*. 2021; 28:112-126.e6.
26. Gris P, Tighe A, Levin D, Sharma R, Brown A. Transcriptional regulation of scar gene expression in primary astrocytes. *Glia*. 2007;55:1145-1155.
27. Sizonenko SV, Kiss JZ, Inder T, Gluckman PD, Williams CE. Distinctive neuropathologic alterations in the deep layers of the parietal cortex after moderate ischemic–hypoxic injury in the P3 immature rat brain. *Pediatr Res*. 2005;57:865-872.
28. Revuelta M, Elicegui A, Moreno-Cugnon L, Buhrer C, Matheu A, Schmitz T. Ischemic stroke in neonatal and adult astrocytes. *Mech Ageing Dev*. 2019;183:111147.
29. Umekawa T, Osman AM, Han W, Ikeda T, Blomgren K. Resident microglia, rather than blood-derived macrophages, contribute to the earlier and more pronounced inflammatory reaction in the immature compared with the adult hippocampus after hypoxia–ischemia. *Glia*. 2015;63:2220-2230.
30. Kreitzer AC, Malenka RC. Striatal plasticity and basal ganglia circuit function. *Neuron*. 2008;60:543-554.
31. Li XJ, Hu BY, Jones SA, *et al*. Directed differentiation of ventral spinal progenitors and motor neurons from human embryonic stem cells by small molecules. *Stem Cells*. 2008;26:886-893.
32. Xiong M, Yang Y, Chen GQ, Zhou WH. Post-ischemic hypothermia for 24 h in P7 rats rescues hippocampal neuron: Association with decreased astrocyte activation and inflammatory cytokine expression. *Brain Res Bull*. 2009;79:351-357.
33. Ziemka-Nalecz M, Jaworska J, Zalewska T. Insights into the neuroinflammatory responses after neonatal hypoxia–ischemia. *J Neuropathol Exp Neurol*. 2017;76:644-654.
34. Chuhma N, Tanaka KF, Hen R, Rayport S. Functional connectome of the striatal medium spiny neuron. *J Neurosci*. 2011;31: 1183-1192.
35. Joesch M, Mankus D, Yamagata M, *et al*. Reconstruction of genetically identified neurons imaged by serial-section electron microscopy. *Elife*. 2016;5:e15015.
36. Wickersham IR, Lyon DC, Barnard RJ, *et al*. Monosynaptic restriction of transsynaptic tracing from single, genetically targeted neurons. *Neuron*. 2007;53:639-647.
37. Guo Q, Wang D, He X, *et al*. Whole-brain mapping of inputs to projection neurons and cholinergic interneurons in the dorsal striatum. *PLoS One*. 2015;10:e0123381.
38. Chen Y, Xiong M, Dong Y, *et al*. Chemical control of grafted human PSC-derived neurons in a mouse model of Parkinson's disease. *Cell Stem Cell*. 2016;18:817-826.
39. Herz J, Koster C, Reinboth BS, *et al*. Interaction between hypothermia and delayed mesenchymal stem cell therapy in neonatal hypoxic–ischemic brain injury. *Brain Behav Immun*. 2018; 70:118-130.
40. Daadi MM, Davis AS, Arac A, *et al*. Human neural stem cell grafts modify microglial response and enhance axonal sprouting in neonatal hypoxic–ischemic brain injury. *Stroke*. 2010;41: 516-523.
41. Comi AM, Cho E, Mulholland JD, *et al*. Neural stem cells reduce brain injury after unilateral carotid ligation. *Pediatr Neurol*. 2008;38:86-92.
42. Dayer AG, Jenny B, Sauvain MO, *et al*. Expression of FGF-2 in neural progenitor cells enhances their potential for cellular brain repair in the rodent cortex. *Brain*. 2007;130(Pt 11): 2962-2976.
43. Park KI, Teng YD, Snyder EY. The injured brain interacts reciprocally with neural stem cells supported by scaffolds to reconstitute lost tissue. *Nat Biotechnol*. 2002;20:1111-1117.
44. Vadivelu S, Platik MM, Choi L, *et al*. Multi-germ layer lineage central nervous system repair: Nerve and vascular cell generation by embryonic stem cells transplanted in the injured brain. *J Neurosurg*. 2005;103:124-135.
45. Grealish S, Diguet E, Kirkeby A, *et al*. Human ESC-derived dopamine neurons show similar preclinical efficacy and potency to fetal neurons when grafted in a rat model of Parkinson's disease. *Cell Stem Cell*. 2014;15:653-665.
46. Eroglu C, Barres BA. Regulation of synaptic connectivity by glia. *Nature*. 2010;468:223-231.
47. Park H, Poo MM. Neurotrophin regulation of neural circuit development and function. *Nat Rev Neurosci*. 2013;14:7-23.
48. Drukker M, Katchman H, Katz G, *et al*. Human embryonic stem cells and their differentiated derivatives are less susceptible to immune rejection than adult cells. *Stem Cells*. 2006;24:221-229.
49. Bradley JA, Bolton EM, Pedersen RA. Stem cell medicine encounters the immune system. *Nat Rev Immunol*. 2002;2:859-871.
50. Piao J, Zabierowski S, Dubose BN, *et al*. Preclinical efficacy and safety of a human embryonic stem cell-derived midbrain dopamine progenitor product, MSK-DA01. *Cell Stem Cell*. 2021;28: 217-229.e7.
51. Cyranoski D. Trials of embryonic stem cells to launch in China. *Nature*. 2017;546:15-16.
52. Schweitzer JS, Song B, Herrington TM, *et al*. Personalized iPSC-derived dopamine progenitor cells for Parkinson's disease. *N Engl J Med*. 2020;382:1926-1932.
53. Mandai M, Watanabe A, Kurimoto Y, *et al*. Autologous induced stem-cell-derived retinal cells for macular degeneration. *N Engl J Med*. 2017;376:1038-1046.